D-A091 612 STATE UNIV OF NEW YORK AT STONY BROOK DEPT OF MATERIA--ETC F/G 11/6
ION IMPLANTATION METALLURGY: A STUDY OF THE COMPOSITION, STRUCT--ETC(U)
APR 80 C R CLAYTON, H HERMAN, K G DOSS N00014-77-C-0424
UNCLASSIFIED TR-2 NL

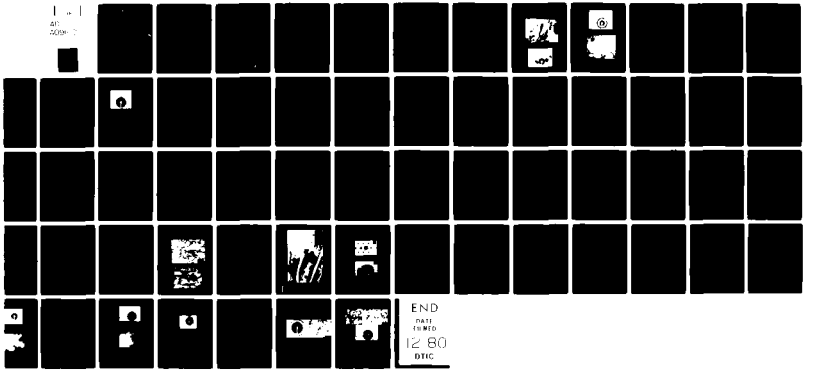

END
DATE FILMED
12 80
DTIC

LEVEL II



# ION IMPLANTATION METALLURGY:

# A STUDY OF THE COMPOSITION, STRUCTURE AND CORROSION BEHAVIOR OF SURFACE ALLOYS FORMED BY ION IMPLANTATION

C. R. Clayton, H. Herman, K. G. K. Doss, W. W. Hu,
S. Prasad and Y. F. Wang

April, 1980



Technical Report No. 2

to

The Office of Naval Research

Contract No. N0001477C0424

(14) TR-2

SECURITY CLASSIFICATION OF THIS PAGE (When Data Entered)

| REPORT DOCUMENTATION PAGE | READ INSTRUCTIONS BEFORE COMPLETING FORM |
|---|---|
| 1. REPORT NUMBER: Technical Report No. 2 | 2. GOVT ACCESSION NO.: AD-A092 612 |
| 3. RECIPIENT'S CATALOG NUMBER | |
| 4. TITLE (and Subtitle): Ion Implantation Metallurgy: A Study of the Composition, Structure and Corrosion Behavior of Surface Alloys Formed by Ion Implantation. | 5. TYPE OF REPORT & PERIOD COVERED: (9) Technical Progress Report. |
| | 6. PERFORMING ORG. REPORT NUMBER |
| 7. AUTHOR(s): (10) C. R. Clayton, H. Herman, K. G. K. Doss, W. W. Hu, S. Prasad and Y-F Wang | 8. CONTRACT OR GRANT NUMBER(s): N0001477C0424 new |
| 9. PERFORMING ORGANIZATION NAME AND ADDRESS: Department of Materials Science and Engineering, State University of New York, Stony Brook, NY 11794 | 10. PROGRAM ELEMENT, PROJECT, TASK AREA & WORK UNIT NUMBERS: (11) AF-NR 840 |
| 11. CONTROLLING OFFICE NAME AND ADDRESS: Office of Naval Research, Department of the Navy, Arlington, VA 22217 (12) 62 | 12. REPORT DATE: April, 1980 |
| | 13. NUMBER OF PAGES |
| 14. MONITORING AGENCY NAME & ADDRESS (if different from Controlling Office): (15) N00014-77-C-0437 | 15. SECURITY CLASS. (of this report): Unclassified |
| | 15a. DECLASSIFICATION/DOWNGRADING SCHEDULE |

16. DISTRIBUTION STATEMENT (of this Report)

Distribution of this document is unlimited

17. DISTRIBUTION STATEMENT (of the abstract entered in Block 20, if different from Report)

18. SUPPLEMENTARY NOTES

19. KEY WORDS (Continue on reverse side if necessary and identify by block number)

Ion Implantation, Passivity, Mechanical Properties, Radiation Effects

20. ABSTRACT (Continue on reverse side if necessary and identify by block number)

See Abstract

DD FORM 1 JAN 73 1473 EDITION OF 1 NOV 65 IS OBSOLETE
S/N 0102-LF-014-6601

4C1074

SECURITY CLASSIFICATION OF THIS PAGE (When Data Entered)

## Abstract

The ion implantation technique ~~has been~~ was used in order to improve the surface mechanical properties and corrosion resistance of iron and steel. Nitrogen implantation ~~has been~~ was found to improve the fatigue lifetime and cavitation resistance of 1018 steel. TEM and internal friction studies ~~have been~~ were carried out in order to determine the nature of this strengthening mechanism. Phosphorous implantation into 304 stainless steel ~~has been~~ was shown to produce a microcrystalline surface alloy saturated with P. Combined electrochemical and XPS studies revealed that the general corrosion of 304 in deaerated 1N $H_2SO_4$ is improved, this effect being due to the formation of a modified passive film.

Finally, a study is reported of the radiation effects resulting from the ion implantation of $As^+ \rightarrow Au$ and $Fe^+ \rightarrow Al$. As(+) yields Au and Fe(+) yields Al. The resulting surface alloys ~~have been~~ were studied using HVEM.

# AN XPS AND ELECTROCHEMICAL STUDY OF THE MODIFICATION OF THE CORROSION BEHAVIOR OF 304 STAINLESS STEEL BY PHOSPHORUS IMPLANTATION


## Abstract

Phosphorus was implanted into 304 stainless steel at a fluence of $10^{17}$ ions $cm^{-2}$ at 40 KeV. The structure of the surface alloy thus formed was found to be microcrystalline, with P in solid-solution. The modification in the corrosion behavior of 304 stainless steel, resulting from P-implantation, was determined from electrochemical polarization experiments carried out in deaerated 1N $H_2SO_4$ and 0.1 N NaCl solution. ESCA was used to characterize the composition and relative thickness of pre-passive layers and the passive film formed at +550 mV vs S.C.E., in order to explain the observed change in corrosion behavior.

## Introduction

It has been shown that when P is an ingredient of low chromium · e-based amorphous alloys, a passive film can be formed having an extremely high chromium content (1,2). Such passive films, based upon chromium oxyhydroxide, result from preferential dissolution of Fe. These alloys show a remarkable corrosion resistance to both general and localized corrosion. Amorphicity in the metallic phase aids in improving the continuity of the passive film, thereby reducing the number of active sites. Indeed, such a high level of Cr enrichment in the passive film could be expected to improve the corrosion resistance of crystalline alloys. It has in fact been demonstrated by Okamoto (3) that Cr enrichment increases the level of bound water in the passive film and that bound water is largely responsible for the repassivation of active sites in the film by hydration of cations and their subsequent incorporation into the lattice.

In this work we have considered the possibility of improving the Cr concentration of the passive films formed on 304 stainless steel, in acid solution, by ion inplantation of phosphorus into the first 100-150Å of the steel to form a solid-solution. The resulting modifications in the active-passive behavior of this steel in 1N $H_2SO_4$ has been studied using electrochemical techniques and ESCA. Pitting studies were also carried out in 0.1 N NaCl solution.

## Experimental

The composition of the 304 stainless steel used in this work is given in Table 1.

Table 1. Composition of 304 Stainless Steel

| % Cr | % Ni | % Mn | % Si | % Mo | % C | % N | % S | % P |
|---|---|---|---|---|---|---|---|---|
| 18.18 | 8.48 | 1.75 | 0.5 | 0.36 | 0.051 | 0.05 | 0.005 | 0.028 |

Coupons of 7x7x1 mm were cut from sheet 304 stainless steel, and were polished up the grades from 600 grit emery cloth to 1 μm diamond paste finish. The

The samples were then sealed in a pre-evacuated quartz tube and annealed at 1100°C for 3 hours followed by water quenching, carried out by breaking the quartz tube under water. The samples were given a final 1 μm diamond paste polish to remove surface oxides and other surface segregants. The samples were then cleaned in methanol and implanted to a fluence of $10^{17}$ ions $cm^{-2}$ at 40 KeV. Ion-thinned 3 mm diameter discs suitable for TEM analysis were also implanted. Heat sinking was achieved by fixing the samples to a copper block.

ESCA Analysis

A V.G. Scientific ESCA 3MKII system equipped with an ion-gun was used to depth-profile the surface alloy. Argon ion-etching was carried out at 2.5 KeV with a current of ~10 μA. The beam was 60° incident to the sample and the background pressure of Ar was $\sim 10^{-6}$ torr during sputtering. Spectra was taken using $AlK_{\alpha 1,2}$ radiation. Following wide-scan analysis of 1000 eV, separate narrow scans were made of the 2p spectra of Fe, Cr, Ni and P and the 1s spectra of C and O.

Depth profiling was carried out to determine the implantant distribution and to monitor any redistribution of the main alloy constituents resulting from selective sputtering or radiation-enhanced diffusion. Fig. 1a shows the variation of P concentration with depth. Fig. 1b shows that beyond the initial region representing removal of the oxide film, no redistribution of the main alloying elements is seen, suggesting that no radiation-enhanced diffusion or selective sputtering occurred during implantation. The concentrations of the elements given in Fig. 1b agree well with the bulk composition of this alloy. In addition, the 2p binding energies of the 2p photoelectron peaks for the four elements considered, showed no signs of a chemical shift indicative of the formation of phosphides.

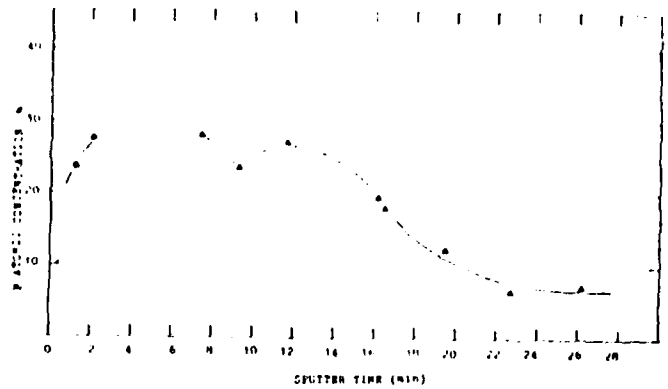

Fig. 1a ESCA Depth concentration profile of Phosphorus in P-implanted 304 Stainless Steel

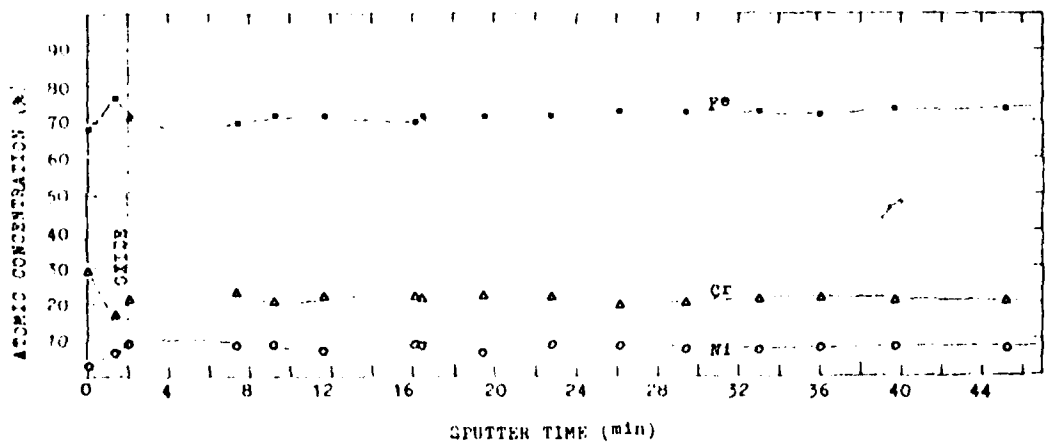


Fig. 1b ESCA Depth concentration profiles of Fe, Cr and Ni corresponding to P-implanted 304 Stainless Steel.

TEM Analysis

The ion-thinned 304 stainless steel sample was examined in a Philips EM300 microscope and the typical microstructure of 304 is shown in Fig. 2a, with the diffraction pattern of this area given in Fig. 2b. The austenitic structure shows some annealing twins and dislocations. On implantation with $P^+$, a dramatic change in structure takes place, which appears from the halo in the diffraction pattern (Fig. 2c) to be indicative of an amorphous or microcrystalline phase. No evidence is found of phosphide formation in this surface alloy. The structure indeed looks amorphous, until at a magnification of 180,000X a very fine grain

structure becomes apparent. Fig. 2d shows a grain size of 50Å in diameter. This result is in contrast to the work of Whitton et al (4), who applied the same implantation conditions in implanting consistent P into 316 stainless steel, in which they report an amorphous structure.

Fig. 2a Micrograph of 304 Stainless Steel Before Implantation

Fig. 2b SAD pattern of 304 Stainless Steel Before Implantation

Fig. 2c Diffraction Pattern of 304 Stainless Steel after 40 KeV $P^+$ Implantation.

Fig. 2d Micrograph of 304 Stainless Steel After 40 KeV $P^+$ Implnatation X 180,000.

## Electrochemical Analysis

Having determined the compositional and structural nature of the implanted steel, electrochemical analysis was carried out to determine how P-implantation modified the general and localized corrosion behavior of 304 stainless steel.

### Polarization Experiments

To study the active-passive behavior, argon saturated 1N $H_2SO_4$, and contained in a conventional polarization cell was used. Analar grade chemicals and double-distilled water were used throughout the experiments. Potentiokinetic sweeps were made at 1 mV $sec^{-1}$. This high rate was used to prevent excessive modification of the surface alloy composition throughout the experiment. Where cathodic pre-treatments were carried out, samples were hydrogen charged for 15 minutes at $10^3$ $\mu A\ cm^{-2}$ which correspond to potentials of -550 to -650 mV (vs SCE). All potentials are stated as measured against the S.C.E.

Anodic polarization was carried out after 5 minutes at Open Circuit Potential (O.C.P.) in the case of the implanted and cathodically pretreated steels and 15 minutes for the unimplanted steel. Samples that were not cathodically pretreated were anodically polarized 5 minutes after immersion.

In localized corrosion studies, anodic polarization at a sweep rate of 1 mV $sec^{-1}$ was carried out in Ar-saturated 0.1 N NaCl solution. Cathodic pretreatment was carried out for 15 minutes at $10^3$ $\mu A\ cm^{-2}$, which was only achieved at potentials in excess of -1.0V. This resulted in an increase of pH which was not corrected. Thus, caution must be made in comparing samples which were cathodically pretreated and those which were not. Buffer solutions were not added, as the buffer process may inhibit natural reductions in pH occurring in pit-solutions (5).

(a) Anodic Polarization in 1N $H_2SO_4$

The anodic polarization diagrams of the implanted and unimplanted samples are shown in Figs. 3 and 4 and corresponding data are given in Table 2.

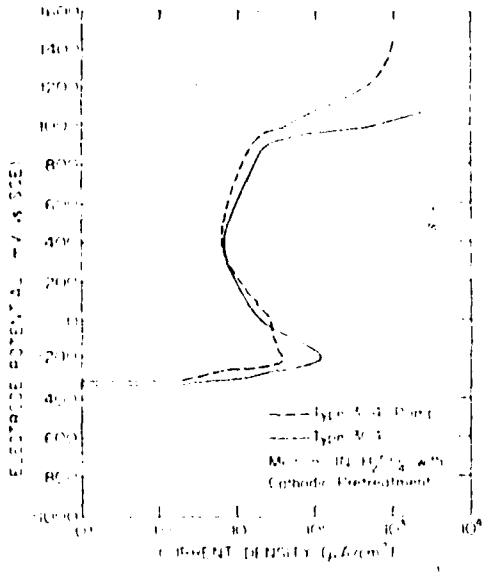

Fig. 3 Anodic polarization curves of 304 stainless steel and $P^+$-implanted 304 stainless steel in 1N $H_2SO_4$ with cathodic pretreatment.

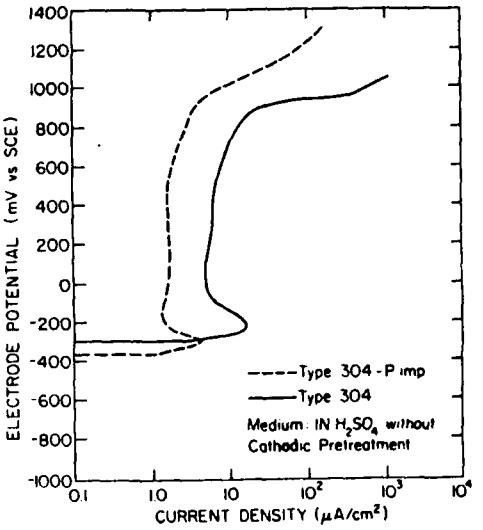


Fig. 4 Anodic polarization curves of 304 stainless steel and $P^+$-implanted 304 stainless steel in 1N $H_2SO_4$ without cathodic pretreatment.

Table 2. Anodic Polarization Parameters Determined in Deaerated 1N $H_2SO_4$

| Material | Cathodic Pretreatment | EOCP (mV vs SCE) | $E_p$ (mV vs SCE) | i crit $\mu A\ cm^{-2}$ | i pass $\mu A\ cm^{-2}$ | $E_T$ |
|---|---|---|---|---|---|---|
| 304 | Yes | -330 | -200 | 120 | 6.8 | 900 |
| 304 | No | -300 | -200 | 16 | 5.0 | 900 |
| $p^+$-implanted 304 | Yes | -320 | -200 | 40 | 6.3 | 940 |
| $p^+$-implanted 304 | No | -364 | -300 | 4 | 1.7 | 960 |

After cathodic pretreatment, the implanted steel shows a substantial reduction in the critical current density (1 crit) by 80 $\mu A\ cm^{-2}$ (Table 2). The passivation potential (Ep) is not changed, however, and a second anodic current maximum

(S.A.C.M.) is found at 0 mV vs SCE. A similar maximum has been observed in the polarization of 304 stainless steel (6). The passive range is almost unchanged by $P^+$-implantation - only above +400 mV is some small improvement seen in the passive current density. However, the transpassive potential ($E_T$) is elevated by 40 mV, and the slope of the curve is increased, indicating some relative reduction in transpassive breakdown; which is a common feature of metallic glasses.

Fig. 4 shows that the anodic kinetics are markedly reduced by the existence of the air-formed films (304 stainless steel has a polish-formed oxide film). The implanted samples studied show a lowering of the passivation potential by 100 mV. Also, the immersion potential is 44 mV more active than the O.C.P. of the cleaned surface. Relative to the 304 stainless steel samples polarized without removal of the oxide film, the phosphorus-implanted samples show a lowering of the passivation potential by 100 mV, and a lower critical current density and passivation current density. In addition to this, the transpassive potential is elevated further to +960 mV.

Fig. 5 is a comparison of the anodic polarization behavior of cathodically pretreated P-implanted 304 stainless steel, after holding for 5 minutes and 30 minutes at O.C.P. The longer periods of exposure to 1N $H_2SO_4$ at O.C.P. were expected to result in gradual corrosion of the surface alloy, exposing a higher level of phosphorus, therefore, enabling a comparison of the two different levels of phosphorus to be made. A second cathodic treatment was carried out in each case to reduce any barrier film products which may begin to develop . It can be seen that the higher phosphorus level resulting in a lowering of the critical current density from 40 to 5.3 $\mu A\ cm^{-2}$ and a reduction of the passive current density from 6.3 to 3.5 $\mu A\ cm^{-2}$. However, the S.A.C.M. became more prominent. The transpassive behavior was seen to revert back to that found for 304 stainless steel, suggesting that at this level of potential the implanted region had been completely removed.

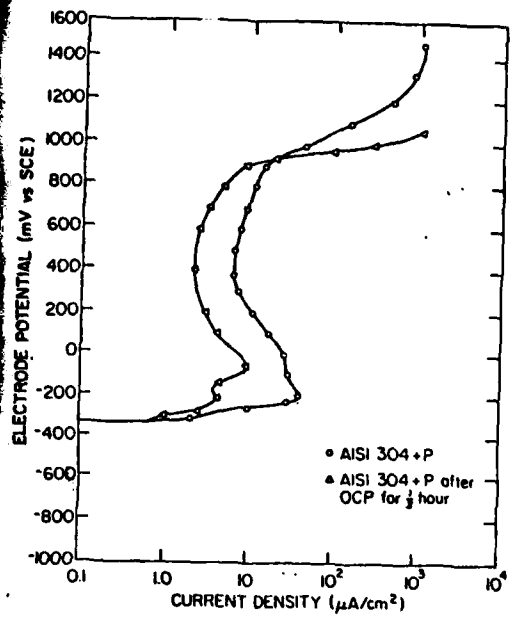


odic polarization curves of $P^+$-implanted
ainless steel in 1N $H_2SO_4$ before and after
e O.C.P. experiment.

n in 0.1 N NaCl Solution

the anodic polarization curves for the implanted and

breakdown potentials and O.C.P. are given in Table 3.

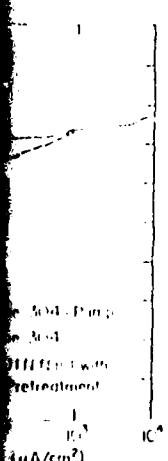

tion curves
s steel and
4 stainless
aCl with
atment.

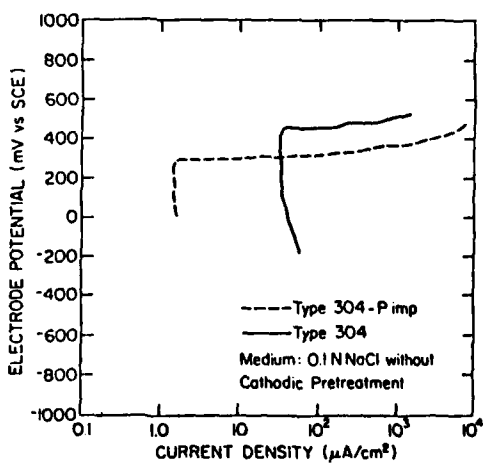


Fig. 7 Anodic polarization curves of 304 stainless steel and $P^+$-implanted 304 stainless steel in 0.1N NaCl without cathodic pretreatment.

Table 3. Anodic Polarization Parameter Determined in Deaerated 0.1 N NaCl.

| Material | Cathodic Pretreatment | EOCP (mV vs SCE) | $i_p$ ($\mu A\ cm^{-2}$) | $E_b$ (mV vs SCE) |
|---|---|---|---|---|
| 304 | Yes | -200 | 60 | +400 |
| 304 | No | -180 | 35 | +460 |
| P-implanted 304 | Yes | -380 | 8.5 | +170 |
| P-implanted 304 | No | 0 | 1.5 | +300 |

It can be seen that regardless of cathodic treatment, the P-implanted steel has a lower resistance to localized corrosion. All of the samples pitted and no evidence of crevice corrosion was observed. This behavior is contrary to what might be expected from the performance of splat-quenched metal glasses. This may be the result of a mixture of amorphous and crystalline phases, or simply resulting from the observed microcrystalline phase. A further possibility is the formation of a passive film having inferior properties to that of 304 stainless steel. At this stage it is necessary to define more clearly the nature of the passive film and pre-passive barrier layer found on the implanted and unimplanted steel and to compare this with observations reported on amorphous metal alloys known to have very high corrosion resistance.

E.S.C.A. Analysis

In this analysis the Fe, Cr, Ni, P, and $S_{2P}$ photoelectron peaks were recorded with the peaks of O1s and C1s. Spectra were taken at two electron take-off angles: 30° and 50° (angles measured from the sample surface). At 30° analysis of the outer layers of the film is enhanced. Assuming a mean-free path of 1.8 nm for the photoelectrons ejected from the $Cr2p^{3/2}$ level, the escape depth measured normal to the surface of the film can be shown to be 1.38 nm at 50° and 0.9 nm at 30° (7).

(a) During TEM analysis of the implanted steel, an outgrowth of oxide was found

at a hole in the sample, and a selected area diffraction pattern was taken. The diffraction pattern is given in Fig. 8. Table 4 summarizes the data, comparing it with the ASTM card index values for the β FeOOH and CrOOH structure.

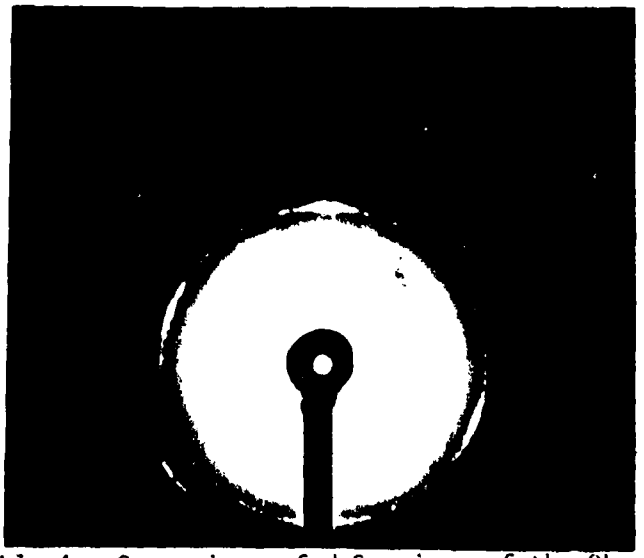

Fig. 8 SAD pattern of the oxide formed on phosphorus implanted 304 stainless steel.

Table 4. Comparison of d-Spacings of the Observed Oxide Layer Formed on P-Implanted 304 with β FeOOH and CrOOH.

| Calculated d-Spacings Å | d-Spacings Å β FeOOH | d-Spacings Å CrOOH |
|---|---|---|
| 3.298 | 3.311 | 3.22 |
| 2.349 | 2.543 (2.285) | 2.434 |
| 1.917 | 1.944 | |
| 1.649 | 1.635 | 1.636 |
| 1.481 | 1.515 (1.438) | 1.480 (weak) |
| 1.352 | 1.374 | 1.345 |
| 1.180 | NA | 1.185 (weak) |
| 1.106 | NA | 1.089 (weak) |

The pattern is seen to closely resemble a mixed Cr-Fe oxyhydroxide structure, since the d-spacings of CrOOH lie within the error associated with the calculated values of d-spacings, i.e., ± 2%. ESCA analysis showed that the oxidized state of Cr was shifted 3.2 eV away from the metallic state in good agreement with CrOOH. The O 1s spectra was a multiplet comprising of almost 50:50 $OH^-$:$O^=$. The Fe $2p^{3/2}$ was in the $Fe^{3+}$ state shifted 3.4 eV away from the metallic signal. The $Ni2p^{3/2}$ was not observed. It is therefore concluded that the film is predominantly composed of $Fe^{3+}$ and $Cr^{3+}$ cations in a CrOOH structure.

The oxide film formed on 304 during polishing was also observed in the microscope, but only one diffracted line was observed. ESCA analysis found evidence of $Fe^{3+}$, $Cr^{3+}$ and $Ni^{2+}$ (minor constituent) and $O^{=}$ with $OH^{-}$. However, this was determined to be a mixture of hydrated $Fe_2O_3$, $Cr_2O_3$ and NiO.

(b) Analysis of Anodically Polarized Samples

Returning to the active-passive behavior of the P-implanted 304, two sets of surface analysis were carried out for each of the four cases depicted in Fig. 3 and 4. Surface analysis was carried out after (a) scanning to the passivation potential and (b) scanning to +550 mV and potentiostating for 1 hour. Potentiostating in the active range would result in changes in the surface alloy composition. Thus, scanning was carried out to stimulate the condition under which Fig. 3 and 4 were produced. Potentiostating at +550 mV resulted in small anodic protection currents which were not expected to alter the alloy composition significantly. The samples were washed in methanol and transferred to the ESCA chamber.

Analysis of Passive Films Formed at +550 mV

The data are presented in Fig. 9-12. Nickel in all cases showed a weak oxidized state. The signal-to-noise ratio was too poor to reproduce here. It can be seen from the spectra that Cr and O show the strongest and most easily interpreted spectra. Variations of electron take-off angle improves the spectral resolution of the oxidized states of metals by removing or lowering the metallic substrate signals. In the case of iron, the metallic peak is so strong as to create too high a background for the oxidized peaks to be resolved clearly. However, in all cases, a $Fe^{3+}$ state is seen. In the absence of spectral deconvolution, we shall limit our discussion to the better resolved chromium and oxygen spectra. Minor constituents of the passive film include $SO_4^{=}$ and an oxidized state of phosphorus (in the implanted steel only). These constituents do not

appear to take part in the film formation as they are of such small concentrations.

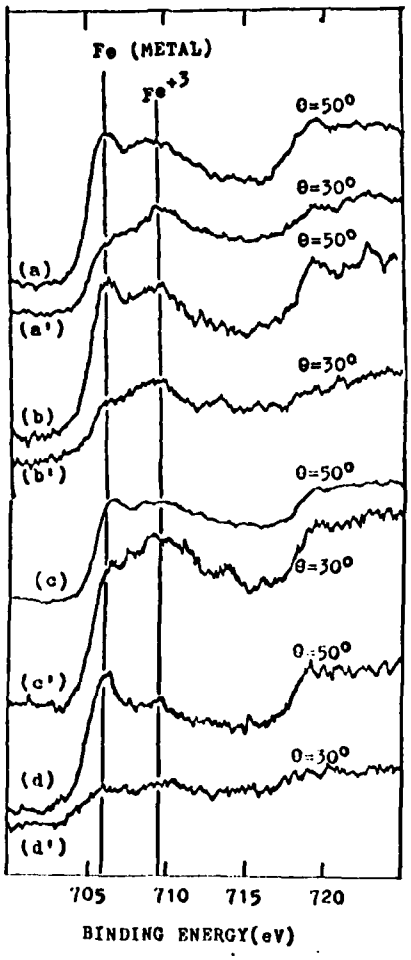


Fig. 9 The Fe 2p spectra measured for specimens passivated in 1N $H_2SO_4$ at +550 mV (SCE) for 1 hr.

(a) and (a'), type 304 with cathodic pretreatment.
(b) and (b'), type 304-P imp. with cathodic pretreatment
(c) and (c'), type 304 without cathodic pretreatment
(d) and (d'), type 304-P imp. without cathodic pretreatment

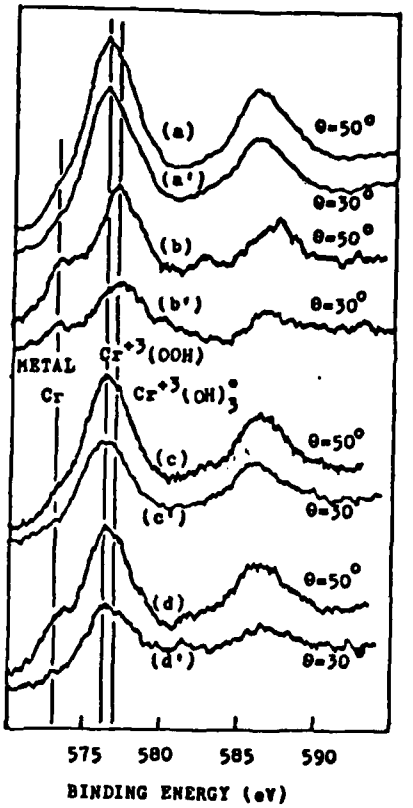


Fig. 10 The Cr 2p spectra measured for specimens passivated in 1N $H_2SO_4$ at +550 mV (SCE) for 1 hour.

(a) and (a'), type 304 with cathodic pretreatment.
(b) and (b'), Type 304-P imp. with cathodic pretreatment.
(c) and (c'), type 304 without cathodic pretreatment.
(d) and (d'), type 304-P imp. without cathodic pretreatment.
*$Cr(OH)_3$ surface charging shift.

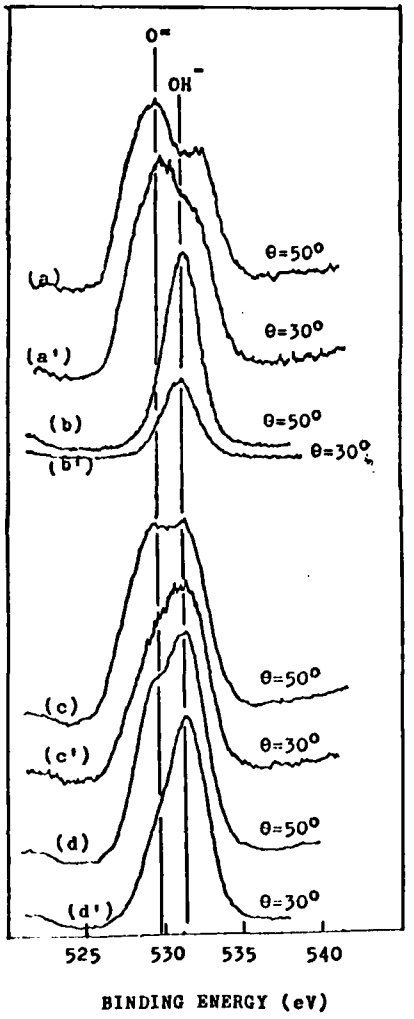


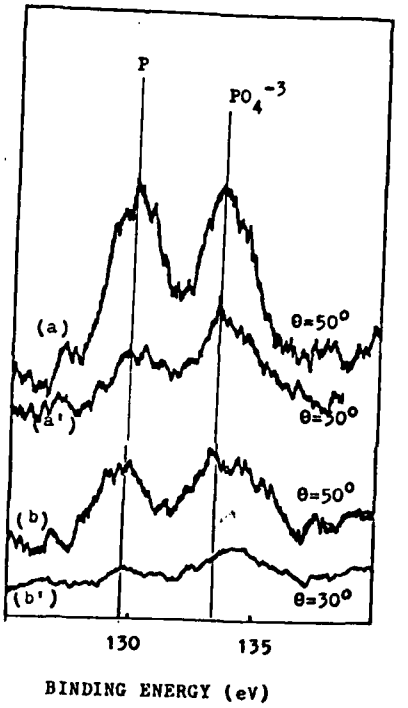


Fig. 11 The O 1s spectra measured for specimens passivated in 1N $H_2SO_4$ at +550 mV for 1 hour.

(a) and (a'), type 304 with cathodic pretreatment.
(b) and (b'), type 304-P imp. with cathodic pretreatment.
(c) and (c'), type 304 without cathodic pretreatment.
(d) and (d'), type 304-P imp. without cathodic pretreatment.

Fig. 12 The P 2p spectra measured for specimens passivated in 1N $H_2SO_4$ at +550 mV (SCE) for 1 hour.

(b) and (b'), type 304-P imp. with cathodic pretreatment.
(d) and (d'), type 304-P imp. without cathodic pretreatment.

It can be seen from the spectra of iron and chromium, that the metallic state is always present at 50°, and this would indicate that these films are

certainly not thicker than the sample depth (i.e., ~1 nm). From the relative height of the metallic signals it can be deduced that in all cases the P-implanted steel produces a thinner film. In addition to this, the samples which were not cathodically pretreated produce a thicker passive film than those that were.

The binding energies of the Cr $2p^{3/2}$ peaks derived from the passiv films formed on 304 stainless steel resemble those of CrOOH. The same shift is observed in the case of P-implanted 304 stainless steel receiving no cathodic pretreatment. However, a further broadening of this peak is seen at higher binding energies. On cathodically pretreating the implanted steel, a very clear shift to higher binding energies is seen. This, however, is associated with an Ols peak, which appears to be almost entirely $OH^-$, but is also shifted to higher binding energies, by as much as 1.1 eV. Charge shifting of $Cr(OH)_3$ has been pointed out by Olefjord and Fischmeiser (8). In Fig. 12 the Ols peak has been repositioned to take account of this charging shift, but this has not been carried out in the case of the chromium peak. Repositioning the chromium peak results in a lower binding energy positon than for CrOOH by 0.45 eV, which corresponds closely to $Cr(OH)_3$ n $H_2O$ Cr $2p^{3/2}$ binding energy. This shift is particularly clear from the 30° spectra. In the sample which was not hydrogen charged, CrOOH is stabilized in the inner layers and in the outer layer, as seen from the 30° spectra, $Cr(OH)_3$ appears as a high binding energy broadening due to selective charging. In addition to this, the $OH^-$ component of the $O^=/OH^-$ multiplet becomes dominant at 30°. It can be seen from the low and braod $Fe^{3+}$ spectral component of the Fe-$Fe^{3+}$ $2p^{3/2}$ multiplet that it is difficult to resolve any similar charge or chemical shift in the iron. At this stage deconvolution of these spectra must remain a future development of this analysis.

We may conclude at this point that an Fe-Cr oxyhydroxide film is naturally formed on 304 stainless steel at the inner layer and some $Cr(OH)_3$ with probably

$Fe(OH)_3$ is produced at the film solution interface. This outer region probably is the precursory stage of the transformation of the film from the hydroxide structure to chromium-enriched oxyhydroxide via the selective dissolution of $Fe^{3+}$.

Anodic polarization of the air-formed film condition in each case produced the above-mentioned, double-layered structure. However, in the case of the P-implanted 304 stainless steel the hydrogen reduction of the air-formed film results in the formation of a single layer structure of Fe, $Cr(OH)_3$.

In the absence of spectral deconvolution it is not possible to give the most precise quantitative analysis of the relative levels of Fe and Cr in the passive films studied. However, an approximate determination can be made from the normalized heights of the multiplets of oxidized state, using previously published sensitivity factors (9). These concentration ratios are given in Table 5.

Table 5. Approximate Concentration Ratios of $Cr^{3+}/Fe^{3+}$

| Materials | Cathodic Pretreatment | Passive Film (+550 mV) | Active Scan |
|---|---|---|---|
| 304 | Yes | 2.3 | 0.6 |
| 304 | No | 4.2 | 0.7 |
| P-implanted 304 | Yes | 1.0 | 0.5 |
| P-implanted 304 | No | 2.0 | 0.8 |

The polarization of the oxidized surface in each case results in approximately twice as much $Cr^{3+}$ to $Fe^{3+}$ in the passive film, than in the pretreated case. In addition, it is seen that for each of the surface conditions studied the unimplanted steel has approximately twice as much $Cr^{3+}$ to $Fe^{3+}$ in the passive film.



(11)

Analysis of the Actively Scanned Samples

This analysis was expected to give some knowledge of the components of the barrier film which will form prior to the main passive film, which at this stage would not be fully developed.

The active scan results in behavior similar to that found in the passive region. Only the spectra for Cr2p is given here, Fig. 13. The cathodically treated samples produce thicker films than for the untreated steels, but generally thickness does not vary much from that found in the passive films. The presence of CrOOH is evident in the barrier films formed on the samples which were not hydrogen charged. The $Cr^{3+}$ to $Fe^{3+}$ ratio is lower than that found in the passive state. These values can be compared in Table 5.

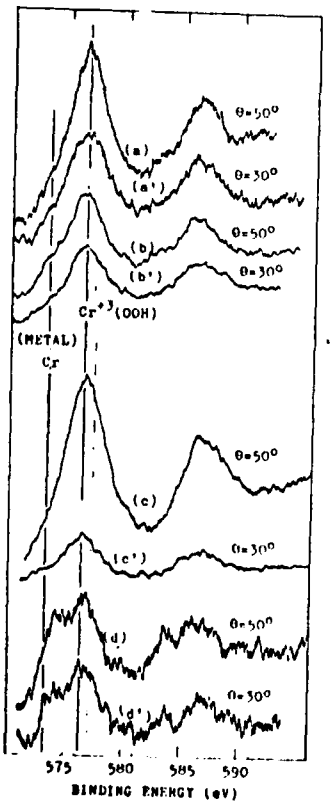


Fig. 13 The Cr 2p spectra measured for specimens actively scanned in 1N $H_2SO_4$.

(a) and (a'), type 304 with cathodic pretreatment.
(b) and (b'), type 304-P Implanted with cathodic pretreatment.
(c) and (c'), type 304 without cathodic pretreatment.
(d) and (d'), type 304-Implanted without cathodic pretreatment.

## Discussion of Results

The modification of the corrosion behavior of 304 stainless steel by implantation with P (40 KeV at $10^{17}$ ions $cm^{-2}$) has been studied by the polarization technique. Subsequent ESCA analysis of the passive films formed on the implanted and unimplanted 304 steel has shown that the composition of the passive film is markedly altered by P-implantation. The passive film of the unimplanted steel consisted of a mixed Fe, Cr oxyhydroxide having a hydrated outer layer, and the implanted steel a mixed Fe, Cr hydroxide. The latter was found to be thinner and to have a lower level of retained chromium.

It has been clearly demonstrated that passive films containing predominantly CrOOH are very stable in acid media (1-2). However, the hydroxide film formed on the P-implanted 304 steel is not so enriched in Cr and indeed is not normally formed on stainless steels. The passivation properties of the hydroxide film formed in the acid media may be attributed to the very highly insulating nature of this film as indicated by the high degree of surface cha ging observed during XPS analysis.

Passive films usually contain bound water in the form of M-OH (hydroxide) or M-O-OH (oxyhydroxide) as in the films studied in this work. Bound water plays an important role in the repassivation of active sites in the film. Okamoto has recently suggested that repassivation is facilitated by the hydration of anodically dissolved metal and subsequent incorporation into the passive film via a bridging bond with the bound water at the nearby passive film surface.(3) However it appears from Okamoto's work that ions can displace "bound water" and produce a soluble metallic chloride complex. When this occurs, incorporation into the lattice of a hydrated cation formed at an active site cannot take place and repassivation is consequently inhibited. Furthermore, it has also been observed that $Cl^-$ ions are able to more easily displace bound water in the form of hydroxide,

compared to oxyhydroxide.[10] This would explain the lower breakdown potentials observed in the case of the cathodically pretreated implanted steel. Since the formation of a passive film containing Fe, Cr OOH is achieved by modification of the air formed film, in this case breakdown potentials in the NaCl solution become more noble. 304 exhibits under these conditions a 60 eV shift in $E_b$ to the more noble direction, whereas, the P-implanted steel exhibits 130 eV shift in the noble direction. This behavior further suggests Okamoto's model of the role of bound water in repassivation.

It could be argued that the vast grain boundary area associated with the microcrystalline surface alloy would result in a high degree of active sites in the passive film since the film would tend to be disrupted at the sites of the underlying grain boundaries. This may be expected to result in a higher overall passive current density. However, the lower current density of the implanted steel in the $Cl^-$ solution would suggest that this is not the case.

Among other preferential sites for pitting are areas of the underlying steel having varying composition. Whereas there is evidence that carbides and other inclusions tend to become partially redissolved under implantation, these sites of differing composition will nevertheless remain, to effect a change in the composition and nature of the normal regions of the passive film. Such chemical heterogeneity is not expected to be present in splat-quenched alloys.

In summary, it would appear that the modified composition of the passive film formed on the P-implanted steel is largely responsible for the lowering of the breakdown potential in $Cl^-$ solution. In the $SO_4^=$ solution the highly insulating nature of the hydroxide type film promotes the passivating character of film. Exactly how P and/or the microcrystallinity of the surface alloy led to the formation of a modified passive film has yet to be elucidated, and remains at present a task for future work.

## Conclusions

1. P-implantation into 304 stainless steel at 40 KeV to fluence of $10^{17}$ ions $cm^{-2}$ results in a microcrystalline surface alloy.
2. The passive film formed on 304 in deaerated 1N $H_2SO_4$ solution after cathodic pretreatment is based upon Fe, CrOOH, whereas the implanted steel passivated at a lower current density forming a passive film based upon Fe, $Cr(OH)_3$.
3. The level of retained chromium in the hydroxide film was significantly lower than for the oxyhydroxide film.
4. The electrically insulating nature of they hydroxide film is believed to be responsible for the good general corrosion resistance of the P-implanted 304 steel.
5. The nature of the bound water in the passive film formed on the implanted steel may be responsible for the lowering of the breakdown potential in $Cl^-$ solution.
6. Polarization after immersion resulted in modification of the existing air-formed film in both implanted and unimplanted steel producing a film based upon CrOOH. Active dissolution involved selective removal of iron to enrich the film with chromium.
7. Improvements in the breakdown potential results were found when no cathodic treatment was carried out.

Acknowledgments

We gratefully acknowledge the financial support of the Office of Naval Research, Arlington, Virginia. We also thank Dr. John Warren of Brookhaven National Laboratory for help with electron microscopy. The equipment support of the National Science Foundation for the purchase of the V.G. ESCA 3MK2 is gratefully acknowledged.

## References

1. K. Asami, K. Hashimoto, T. Masumoto and S. Shimodaira, Corros. Sci. 16, 909 (1976).

2. K. Hashimoto, M. Naka, J. Noguchi, K. Asami and T. Masumoto. Passivity of Metals, Ed., R. P. Frankenthal and J. Kruger (Proc. of Fourth Int. Syp. on Passivity, 1977) p. 156. Pub. Electrochemical Soc. Inc., Princeton, N.J. (1978).

3. G. Okamoto, Corros. Sci. 13, 471 (1973).

4. J. L. Whitton, W. A. Grant and J. S. Williams, Proc. Int. Conf. on Ion Beam Modification of Materials, Budapest, Hungary (1978).

5. J. R. Galvele, Passivity of Metals, Ed. R. P. Frankenthal and J. Kruger, p. 285. Pub. Electrochemical Soc. Inc., Princeton, N.J. (1978).

6. N. D. Greene and R. B. Leonard, Electrochimica Acta., Vol. 9, 45 (1964).

7. M. Klasson, A. Berndtsson, J. Hedman, R. Nilsson, R. Nyholm and C. Nordling, J. Electron. Spectrosc., 3, 427 (1974).

8. I. Olefjord and H. Fischmeister, Corros. Sci., 15, 697 (1975).

9. J. E. Castle and C. R. Clayton, Passivity of Metals, Ed., R. P. Frankenthal and J. Kruger, p. 714, Pub. Electrochemical Soc. Inc., Princeton, N.J. (1978).

10. H. Saito, T. Shibata and G. Okamoto, Corros. Sci. 19 693 (1979).

## Papers Published

1. Interpretation of Electrochemical Behavior of Nickel-Implanted Type-430 Stainless Steel Using XPS and TEM.

   S. B. Agarwal, Y-F Wang, C. R. Clayton, H. Herman and J. K. Hirvonen.
   Thin Solid Films 63(1979) 19-25.

2. Modification of the Corrosion Behavior of 304 Stainless Steel by Phosphorous Implantation.

   C. R. Clayton, K. G. K. Doss, W. Herman, S. Prasad, Y-F Wang, J. K. Hirvonen and G. K. Hubler.
   To be Published in Proc. Materials Research Soc. Meeting, Boston, 1979.

ce-Related Mechanical Properties of

Nitrogen-Implanted 1018 Steel

e-1018 steel (0.18 wt.% carbon) with 75 KeV-nitrogen
modification of fatigue, cavitation-erosion and
data suggests that the modification of surface-related
1018 steel is related to the interactions of nitrogen
igh-cycle fatigue lifetime of N-implanted 1018 steel
ncreased when implanted samples are thermally aged
rstitial migration to and association with near-surface
ion has also been found to improve the cavitation resis-
stilled water. These studies have been accompanied by
explore the responsible mechanisms. An evaluation of
interaction has been made using highly sensitive internal
Other supportive studies using scanning and transmission
ll as nuclear reaction depth profiling are discussed.

## Introduction

Ion implantation of nitrogen has been employed to beneficially modify the surface-sensitive mechanical properties of steels(1-4). The modified properties include: wear, fatigue, and cavitation-erosion. There is evidence that near-surface dislocations interact in some way with the products of the implantation process, the former presumably being impeded in their motion. Such effects are most likely to occur in fatigue and cavitation-erosion which are strongly sensitive to very mear surface effects.

This paper will review our efforts in nitrogen-implantation surface strengthening of AISI 1018 steel (0.18 wt.% C). In addition, we shall present new results, using internal friction, transmission electron microscopy and nuclear reaction depth profiling, which will aid in elucidating this important surface strengthening process.

## Materials and Methods

A commercial 1018 steel, in the form of 9.5 mm diameter rods, was the starting material. The mean grain diameter measured on the cross-section was estimated to be 30 μm, the pearlite percentage being approximately 12%. Chemical analysis gave the following concentrations (in wt.%) of the minor constituents: C(0.15-0.20); Mn(0.6-0.9); P(0.04); S(0.05).

All implantations were carried out utilizing a 150 KeV $(N_2)^+$ molecular beam resulting in 75 KeV implanted nitrogen ions. Unless noted, fluences of $2 \times 10^{17}$ nitrogen atoms/$cm^2$ were used with a dose rate of approximately 25 μA/$cm^2$ and with target temperatures estimated to be under 70°C. These implantation parameters yield a maximum nitrogen concentration of approximately 30 at.%, located at a depth of 80 nm.

## Fatigue and Cavitation-Erosion

Following the pioneering work at Harwell on ion-implantation - modified

surface properties (1), we sought to carry out detailed studies of the effects of nitrogen implantation on fatigue lifetime. We were specifically interested in low stress (high cycle) fatigue tests at ambient temperature (2,3). The fatigue tests were carried out in a rotating beam mode at 5000 RPM, and at a 345 MPa stress level, which is 90% that of the yield stress.

The results of these early studies are shown in Fig. 1, which is a schematic representation of the number of cycles to failure for different treatments. While the as-implanted specimen shows a slight increase in lifetime, a dramatic increase is shown for specimens which are aged following implantation, either artificially (100°C for 6 hours) or naturally (23°C for 16 weeks). In fact, for the majority of the specimens which were aged subsequent to implantation, no failure was observed for $10^8$ cycles. This result represents an improvement of at least two orders of magnitude over that observed for non-implanted specimens. The effect of compressive stress and radiation-induced defects resulting from high-dose implantation was tested by implanting an inert gas, Ne, to comparable depths and concentrations in a fatigue sample. An improvement (i.e., 2X-3X) in the lifetime of this aged sample was seen, however, this is substantially lower than for N.

The cavitation-erosion studies were carried out in distilled water (3). The test for evaluation of this property involves the rapid formation and collapse of a high density of small bubbles near the surface to-be-tested (5,6). The bubbles are formed by the rapidly moving tip of an exponential horn operating at 20 KHz, and at a displacement of 50 μm. The 1.27 cm diameter steel specimen was situated 0.64 mm from the vibrating tungsten carbide tip. To determine the effects of cavitation-erosion, the specimen was intermittently removed and weighed. In addition, SEM studies were carried out along with the weight-loss studies.

Results for three specimen conditions are shown in Fig. 2, where total

weight-loss in mg is plotted versus time of cavitation. It is seen that there appears to be an incubation time of about 45 minutes prior to a large weight loss for the aged specimen, whereas only several minutes of delay is obtained prior to cavitation damage for both the unimplanted and the implanted-only specimens. It should be noted that the total weight-loss and the rate of weight-loss all show similar values beyond the initial period of weight loss (7). Of central importance, however, is the increase in incubation time by at least an order for the implanted and aged specimen prior to the observation of significant cavitation-induced weight-loss.

SEM studies during cavitation-erosion reveal a pattern similar to that seen for the weight-loss measurements. In Fig. 3 are shown two surfaces after 45 minutes of cavitation in distilled water for an untreated specimen (3a) and one that was implanted-and-aged (3b). The mechanical surface distortions are much more developed in Fig. 3a than in 3b. This stage of cavitation, Fig. 3a, looks very much like a specimen which was implanted but not aged.

Internal Friction

Internal friction is a measure of the energy dissipated during cyclic stressing of a meterial (8). It is of interest because it provides information about the processes which occur during fatigue cycling. The data obtained from such measurements are, therefore, complementary to TEM observation and nuclear reaction profiling discussed below, which serve to characterize the condition or state of the specimen at any point in time. Reported here is a preliminary investigation of the internal friction in the unimplanted, implanted, and aged conditions of 1018 steel.

If a reed is allowed to vibrate freely in a vacuum, the amplitude of the vibrations will gradually decrease due to the absorption of energy by processes

such as interstitial diffusion and dislocation motion. When the period of the mechanical vibration is equal to $2\pi$ times the relaxation time of a loss process, the energy absorbed by that loss mechanism is a maximum. Since the relaxation time depends on the temperature, a plot of internal friction as a function of temperature consists of a sequence of loss peaks each of which is indicative of a particular loss mechanism. In principle, the activation energy for each process can be determined from either the width of its loss peak or the shift in temperature at which the peak occurs if the vibration frequency is changed.

Since the mechanisms which contribute to fatigue failure are inherently irreversible, they can reasonably be expected to possess corresponding loss peaks. Thus, in principle, the influence of N-implantation and aging on fatigue lifetime can be studied by establishing which loss peak (and therefore which process) is affected. The purpose of our preliminary investigation was to establish whether, in fact, N-implantation and aging produces observable changes of internal friction.

Two different techniques were used to measure the losses due to internal friction. The width of the curve giving the amplitude of vibration as a function of driving frequency was measured and, in this case, the internal friction, $Q^{-1}$, is given by $(f_2-f_1)/f_2$ where $f_2$ and $f_1$ are the frequencies, at either side of resonance, at which the amplitude is 0.707 the amplitude at the mechanical resonant frequency, $f_0$. The second technique makes use of the fact that the loss is related to the number of cycles executed while the amplitude is allowed to decay to $e^{-1}$ of its initial value through the equation $Q = N\pi$. The resonance width determination was used during the initial phase of the experiment because it required considerably simpler instrumentation. The free decay method was used later because it is orders of magnitude faster, which is a necessary feature if the determination of loss as a function of temperature is to be completed in a

reasonable time. It is noteworthy that the experimental uncertainty was also reduced by nearly two orders of magnitude by using the free decay method.

At the heart of any internal friction apparatus is the sample holder since losses produced by gripping the sample can easily equal or exceed those to be measured. The holder and sample geometry used were constructed following the design of MacCrone (9) and have previously been used by him to measure losses in the order of $10^{-6}$. Since the losses observed in this system were all greater than $10^{-4}$, the contribution due to the holder is negligible.

The reed was driven into vibration at approximately 1 KHz by an alternating current applied to an electromagnet located next to the tip of the reed which had a small piece of ferrite glued to it. The amplitude of vibration was detected by using the motion of the reed to vary the capacitance of an RC circuit with a constant potential. The resultant currents to the capacitor were detected as a voltage across the resistor. A crude measure of the absolute vibration amplitude, and hence the strain, was obtained by measuring the deflection of a laser beam reflected from the reed when it was forced to execute large vibrations. The resulting plot of amplitude as a function of detected signal was then extended to the low vibration amplitudes used during the experiments. From these measurements it was concluded that the strain was less than $10^{-5}$ during the internal friction measurements.

The results of our initial experiments (see Table I) show that the internal friction is reduced, relative to its initial value, by approximately 0.6 and 0.5 following N-implantation and aging, respectively. The values were obtained at room temperature, under a vacuum of approximately $10^{-2}$ torr. These results were repeatable despite the fact that the measurements for the unimplanted and implanted conditions were made on different samples. Moreover, the implanted samples were subjected to considerable handling since the implantations and internal friction

measurements were conducted in different laboratories.

In order to eliminate any deleterious effects from sample handling and to avoid comparing the unimplanted state of one sample with the implanted state of another, subsequent experiments were conducted in-situ. An apparatus was constructed for in-situ measurements which had provisions for rotating the sample so that both sides could be implanted. This apparatus also was equipped with heating and cooling elements so that the internal friction could be measured as a function of temperature.

For the in-situ experiments, $Q^{-1}$ was measured as a function of temperature before and after implantation and following aging. (See Fig. 4) In addition, the dose dependence of $Q^{-1}$ at room temperature was measured and $Q^{-1}$ was found to decrease linearly with the log of the fluence, between $10^{14}$ N/cm$^2$ and $10^{17}$ N/cm$^2$. Even the smallest fluence caused a reduction of approximately 6% in $Q^{-1}$.

The large change in $Q^{-1}$ observed following implantation implies that either (i) the starting material had an inhomogeneous distribution of loss mechanisms with the majority located within the range of the implanted nitrogen, or (ii) that the implanted layer inhibits loss mechanisms far beneath it. Since the starting material was originally mechanically polished, it is expected to have a work-hardened surface. However, this disturbed region extends much farther into the bulk than does the implanted layer. This suggests that loss mechanisms beneath the implanted layer are inhibited by the implanted nitrogen. If, for example, the dominant loss mechanism were dislocation motion, then the pinning of dislocations within the implanted layer must be retarding the motion of dislocations within the bulk. Experiments directed at confirming this hypothesis are underway.

The flat region in the curve of $Q^{-1}$ vs temperature for the unimplanted case is characteristic of a superposition of a number of loss peaks differing slightly

in activation energy. If it is assumed that this broad peak is due to the motion of dislocations, then the observed reduction in loss following implantation can be interpreted as being due to dislocation pinning. Similarly, the further reduction of peak height following aging would be due to an increase in the density of pinning sites. Either the presence of precipitates or the decoration of dislocations by the implanted nitrogen could cause pinning. However, the decoration mechanism of pinning should produce a marked strain dependence in the loss. While the strains imposed during these measurements were kept low to establish a baseline for comparison with future data and the literature, the strain dependence is currently being studied and will be reported elsewhere.

It has been shown that internal friction is extremely sensitive to nitrogen implantation into 1018 steel. The qualitative features of the plot of loss vs. temperature suggest that the reductions of internal friction following implantation and following aging may be due to dislocation pinning. In contrast to the fatigue results, the largest change in behavior was observed immediately following implantation and only a relatively small change occurs after aging. However, this behavior may be reflective only of the low strains imposed during the loss measurements.

Transmission Electron Microscopy

Samples for transmission electron microscopy were prepared for ion implantation from slices spark-cut from the same starting material as used in fatigue tests. These discs were lapped to 0.15 mm and polished with 0.1 μm diamond paste. N-implanted samples were jet thinned from the back side using a solution of perchloric acid, ethanol, and glycerine. It was found that great care must be taken during the electropolishing to avoid unnecessary exposure of the implanted layer to the electrolyte since these layers tend to etch very rapidly.

Microscopy was performed on the unimplanted, as-implanted, and implanted-and-aged states with emphasis on the induced changes in the ferrite ($\alpha$) rather than the carbide phase. Examination of the unimplanted state in bright field (see Fig. 5a) revealed a high density of dislocations in the ferrite and carbide phases in addition to well developed dislocation walls between subgrains. After implantation, the defect density was so large that individual dislocations were difficult to resolve. The electron diffraction pattern of the ferrite grains of all implanted samples, including aged ones, contained extra spots. Analsis of these non-ferrite spots revealed a structure consistent with the metastable iron nitride, $Fe_{16}N_2$ ($\alpha$" in the nomenclature of Jack (10)). Figure 5b is a typical pattern obtained from an implanted sample, showing that the $\alpha$" phase has nucleated with a preferential orientation relative to the phase (the faint spots are due to the " phase). Dark field imaging of the $\alpha$" phase shows a large density of small precipitates uniformly distributed in the ferrite. In the as-implanted state, (see Fig. 5c) the typical precipitate size is estimated to be 10 nm. In addition to the as-implanted distribution of precipitates, the aged samples contain smaller precipitates presumably nucleated during aging. Aged specimens showed contrast features resembling acicular martensite. However, the presence of martensite could not be confirmed due to the interference of overlapping matrix spots (which are already broadened due to the presence of $\alpha$" and double diffraction spots).

In summary, the microstructural changes observed following N-implantation include a large density of defect structures and small precipitates of $Fe_{16}N_2(\alpha")$. Although there exists some evidence of martensitic transformation in aged specimens, the major difference between the aged and the as-implanted states is that the aged samples contain additional, smaller $\alpha$" precipitates.

Nuclear Reaction Profiling

The depth concentration profiles of the implanted nitrogen were measured utilizing the $^{14}_{7}N(d,\alpha)\ ^{12}_{6}C$ nuclear reaction in combination with a high-resolution magnetic spectrometer to energy-analyze the emitted particles. Since the particles lose energy while exiting from the host lattice, the measured energy spectra can be interpreted as inverted depth concentration profiles of the implanted nitrogen (i.e., the highest energy alpha particles originate from interactions with the nitrogen closest to the surface). The nitrogen distribution for the as-implanted sample appeared reasonably symmetric and buried at a depth of about 80 nm with a peak concentration of approximately 30 at.%.

There was little difference observed in the depth distribution profiles of an as-implanted nitrogen sample and the same sample thermally aged for 200°C (20 min) indicating that the nitrogen which is not in precipitate form is presumably being trapped by radiation induced damage. This is in agreement with the findings of Longworth and Hartley (11).

However, samples that had undergone mechanical stress did show significant redistribution of the nitrogen towards the surface, presumably due to stress-induced diffusion. This redistribution was seen in a sample that was aged (23°C for 16 weeks) and showed much longer lifetime as well as for a sample that was freshly implanted and showed no significant increase in lifetime, relative to unimplanted samples.

In summary, aging has no gross effect on the redistribution of implanted nigrogen, and within the sensitivity of our measurements no significant loss of nitrogen from the implanted region was observed.

Discussion

The results of these experiments serve to emphasize the profound influence of the near surface on the macroscopic behavior of metals. We have established that fatigue lifetime can be extended by more than two orders of magnitude and

and the onset of cavitation erosion can be substantially retarded by treating only the first 100 nm of the surface of 1018 steel. While our understanding of the source of these improvements is incomplete, considerable insight into the nature of the effect has been gained. The TEM study has shown that both the as-implanted and aged specimens have qualitatively similar microstructures. In fact, the decomposition of the nitrogen-implanted solution is similar to that found in conventionally prepared nitrided ferrite (12). The major differences between the implanted and conventional alloys are that the $\alpha''$ precipitates are smaller and more dense and the density of defects is greater in the implanted alloy. In addition, the only observable difference between the as-implanted and aged states is the increased number of small $\alpha''$ precipitates. Thus, while the nitrogen is important, (e.g., implanted Ne was found to have little effect on fatigue lifetime) the role played by the nitrides it forms seems to be minor. The nuclear reaction profiling indicates that aging does not cause significant migration of nitrogen from the implanted layer. Yet the internal friction results strongly suggest that the material beneath the implanted layer is affected.

One way to account for these observations is to assume that a process similar to strain aging is occuring. In this interpretation, the implanted nitrogen interacts with defects (either pre-existing or irradiation induced) in such a way as to inhibit the motion of dislocations. However, the required interaction proceeds at a low rate and thus requires several weeks at room temperature or several hours at 100°C. Since the implantation is conducted at 100°C and since ion beam mixing would tend to disorder these stabilizing structures, no improvement is observed for the as-implanted state.

## References


1. G. Dearnaley and N. E. W. Hartley, "New Uses of Ion Implantation", AERE-R 8562, October, 1962; N. E. W. Hartley, "Appl. of Ion Beams to Materials", Conference Ser. No. 28, (1976), 210.

2. W. W. Hu, C. R. Clayton, H. Herman, and J. K. Hirvonen, Scripta Met. 12, 697 (1978).

3. H. Herman, W. W. Hu, C. R. Clayton, J. K. Hirvonen, R. Kant, and R. K. MacCrone, Proc. "Ion Plating and Allied Techniques", London, 3-5 July, 1979, Spectrum Printing Company, Edinburgh.

4. G. Dearnaley, "Practical Applications of Ion Implantation", this volume.

5. R. T. Knapp, J. W. Daily, and F. H. Hamitt, CAVITATION, McGraw-Hill, New York, 1970.

6. EROSION, Ed. C. M. Preece, Vol. 16 (Treatise on Materials Science & Technology), Academic Press, New York, 1979.

7. W. W. Hu, C. R. Clayton, H. Herman, and J. K. Hirvonen, to be published.

8. A. S. Nowick and B. S. Berry, AN ELASTIC RELAZATION IN CRYSTALLINE SOLIDS, Academic Press, New York, 1972.

9. W. W. Scott and R. K. MacCrone (1968b). Rev. Sci. Instr. 39, 821.

10. K. H. Jack, Proc. Roy. Soc. London 308 (1951) 216.

11. G. Longworth and N. E. W. Hartley, Thin Solid Films 48 (1978) 95.

12. A. S. Keh and H. A. Wriedt. Trans. AIME 224 (1962) 650.

## Papers Published

1. "Fatigue-Life Enhancement by Ion Implantation", W. W. Hu, C. R. Clayton, H. Herman and J. K. Hirvonen, Scripta Meta. 12 (1978) 697.

2. "Fatigue-Life Enhancement by Ion Implantation", W. W. Hu, C. R. Clayton, H. Herman and J. K. Hirvonen, Proceedings of IBMM, Budapest (1978).

3. "Modification of Mechanical Properties through Ion Implantation", H. Herman, W. W. Hu, C. R. Clayton, J. K. Hirvonen, R. Kant and R. K. MacCrone. Ion Plating and Associated Techniques, London, July, 1979.

4. "Surface-Related Mechanical Properties of Nitrogen-Implanted 1018 Steel", H. Herman, W. W. Hu, C. R. Clayton, J. K. Hirvonen, R. Kant, R. K. MacCrone and J. A. Kozubowski. Materials Research Society Conference, Boston, November, 1979.

5. "Cavitation-Erosion of Ion-Implanted 1018 Steel", W. W. Hu, C. R. Clayton, H. Herman and J. K. Hirvonen. Materials Science and Engineering, (1980)

6. "Fatigue-Life Enhancement by Ion Implantation", Finommechanika Mikrolechnika, Hungarian, (1980).

## Figure Captions

Figure 1 Fatigue Lifetimes for Different Treatments.

Figure 2 Weight loss during cavitation erosion of 1018 steel. The curves represent (1) the unimplanted condition, (2) N-implanted and (3) N-implanted and aged (10°C for 6 hrs.).

Figure 3 SEM micrographs following 45 minutes of cavitation erosion: (a) unimplanted, (b) N-implanted.

Figure 4 Internal friction as a function of temperature at approximately 1 KHz for the unimplanted, N-implanted, and aged (1 hr. at 130°C) conditions of 1018 steel.

Figure 5 (a) Bright field transmission electron micrographs of the unimplanted state. (b) Electron diffraction pattern of N-implanted sample. The large spots are due to reflections from the ferrite matrix and the small ones are from $Fe_{16}N_2$ precipitates. (c) Dark field micrograph of N-implanted condition using the reflection circled in Figure 5b.

l Friction of Steel Measured at Room Temperature

| le Condition | $Q^{-1}$ (x $10^{-3}$) |
|---|---|
| ved | 1.68 |
| g Implantation | 0.98 |
| g Implantation g at 100°C for | 0.84 |

INFLUENCE OF SPECIMEN TREATMENT ON FATIGUE LIFETIME

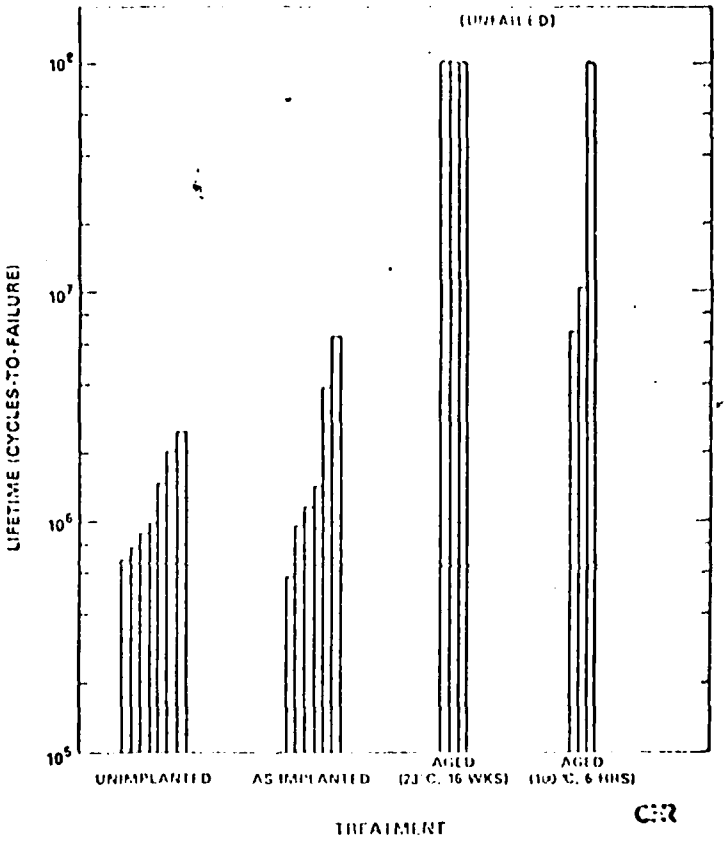


Fig. 1

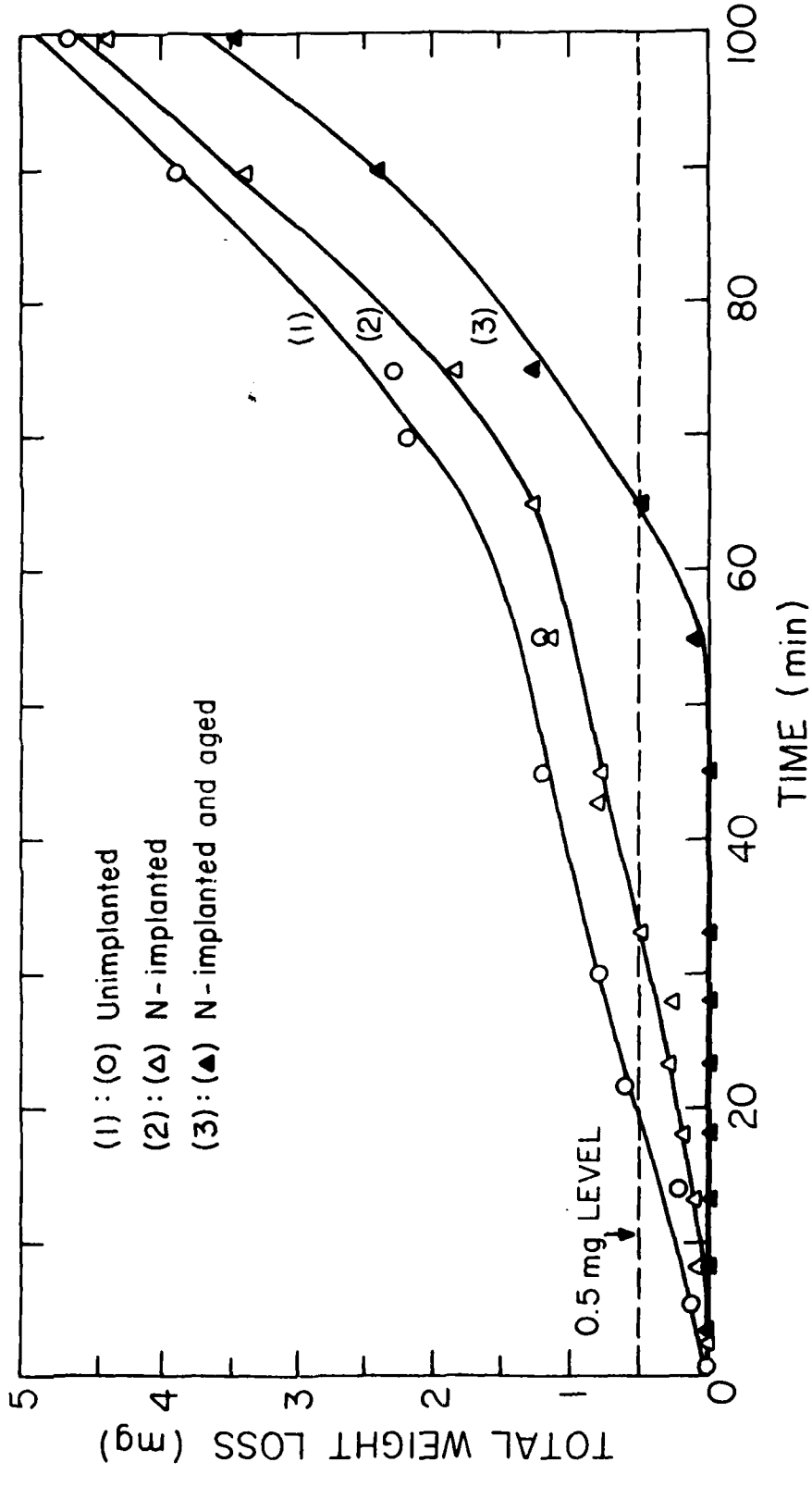
TOTAL WEIGHT LOSS (mg)
TIME (min)
0
1
2
3
4
5
20
40
60
80
100
0.5 mg LEVEL
(1) : (○) Unimplanted
(2) : (△) N-implanted
(3) : (▲) N-implanted and aged
(1)
(2)
(3)

Fig. 2

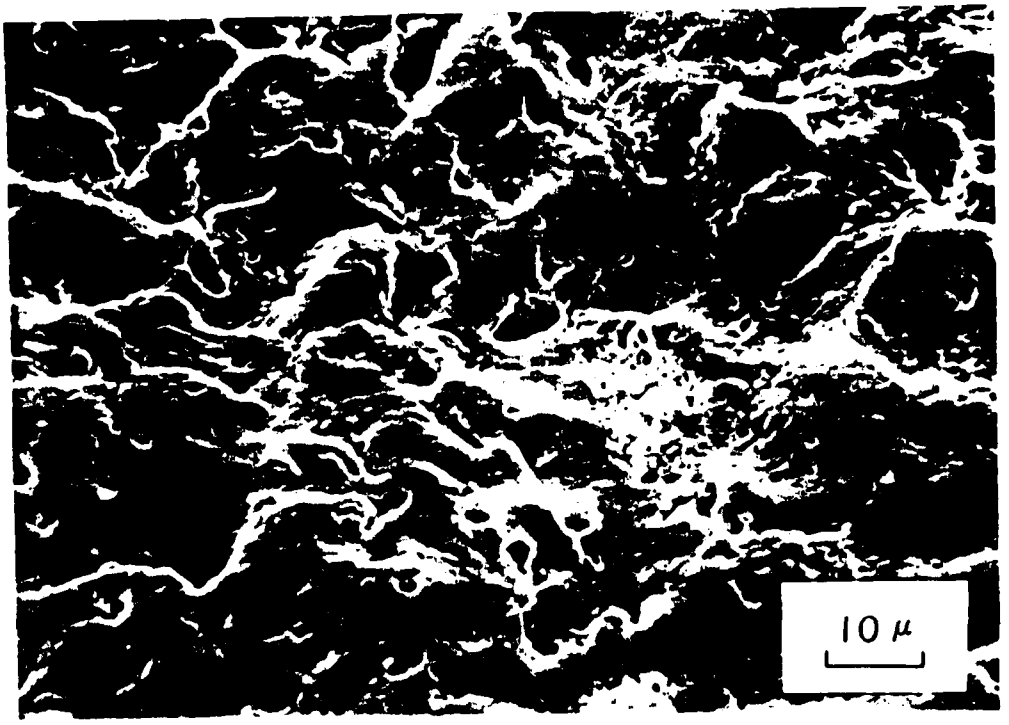


Fig. 3a

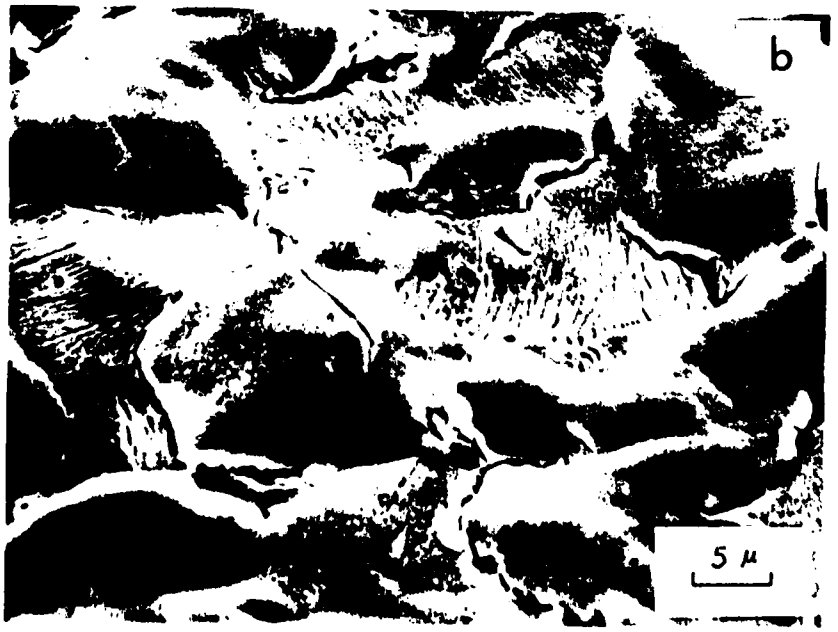


Fig. 3b

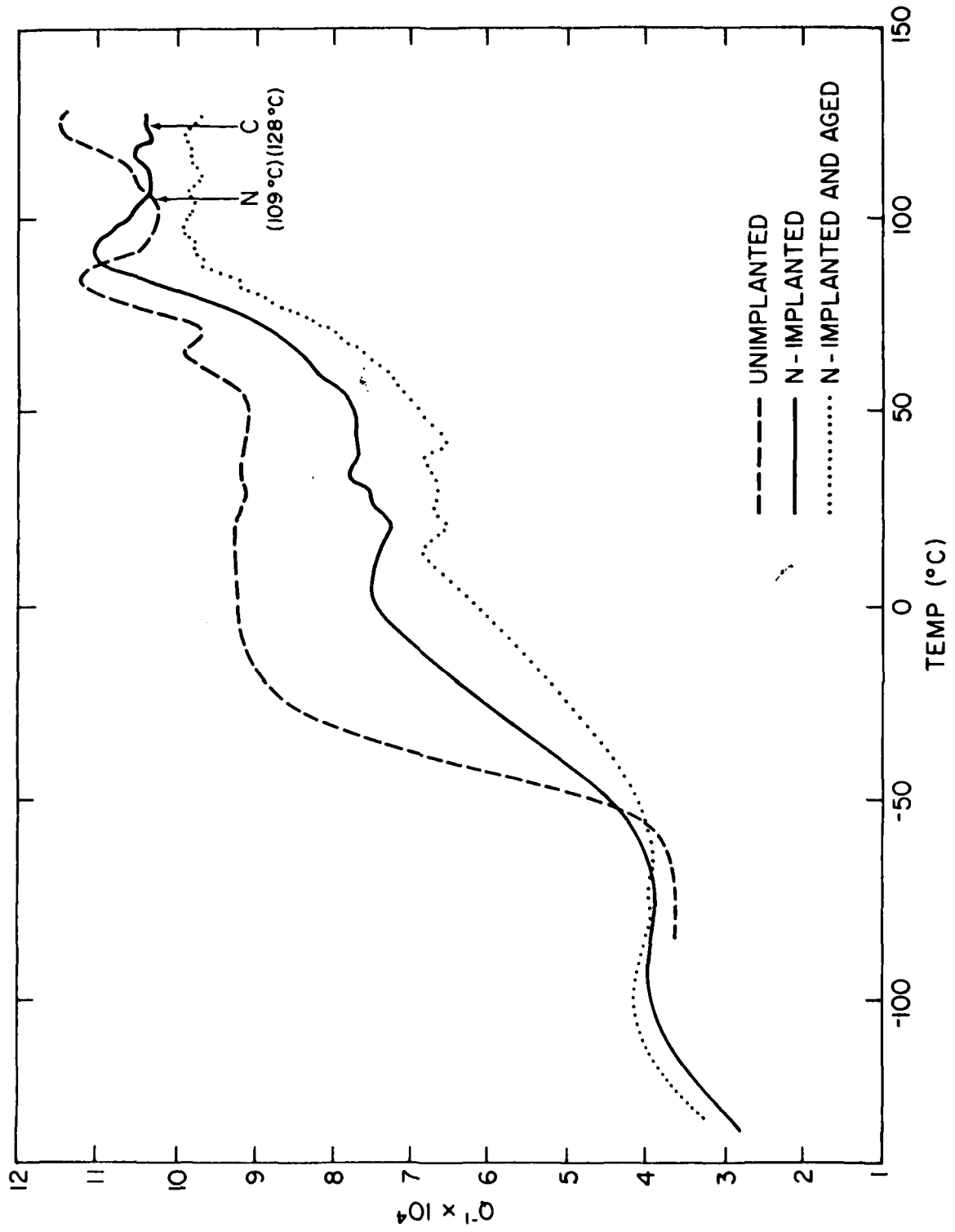
UNIMPLANTED
N-IMPLANTED
N-IMPLANTED AND AGED
C
N
(109 °C)(128 °C)
TEMP (°C)
150
100
50
0
-50
-100
σ⁻¹ x 10⁴
12
11
10
9
8
7
6
5
4
3
2
1

Fig. 4


Fig. 5a

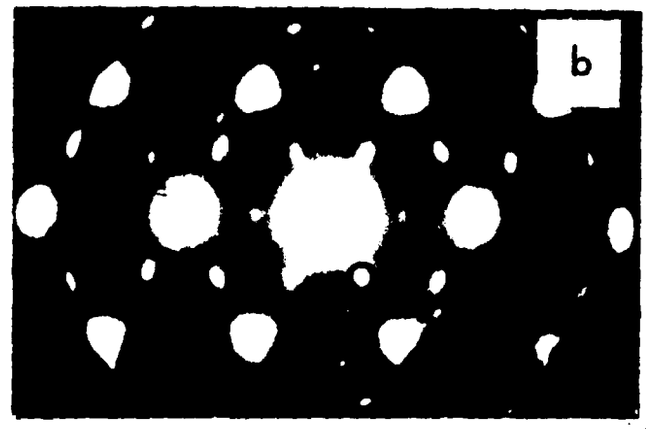


Fig. 5b


Fig. 5c

# ARSENIC IMPLANTATION - INDUCED AMORPHICITY IN GOLD

Ion implantation has been shown to produce highly metastable phases similar to those formed by ultra-rapid quenching of molten alloys (1-3). This has both fundamental and practical significance, especially since, apparently, amorphous surface phases have been generated in this manner (2). Of the amorphous surface-alloys which are formed by the implantation technique most have been formed with an implantant which is a metalloid ion (4,5).

As a part of a program to study amorphous phases by metalloid ion implantation in metals, we examined the implantation of $As^+$ into Au. Based on a number of theories and liquid quenching experiments, an amorphous surface layer was expected (4). Conventional TEM observations (100 KeV), however, showed no evidence of amorphicity, but rather indicated equilibrium crystalline phases at a depth range of approximately 500Å. Based on theoretical calculations we suspected that an amorphous layer was in fact, formed deeper within the Au target, but, subsequently removed by ion thinning from the back of the target. This was confirmed by a high voltage transmission electron microscopic (HVTEM) study on the specimen. A novel situation has thus been encountered in these experiments, where an amorphous layer is embedded deeply within a polycrystalline matrix.

According to the Au-As equilibrium phase diagram there is no mutual solid solubility of As and Au (6), though, due to experimental difficulties, no studies have been made at low concentrations of As. X-ray diffraction showed no solid solubility at higher concentration (greater than 5 at%) and no Au-As compound has been observed. Since ion implantation is a non-equilibrium process, our goal was to determine to what degree a metastable solid solution could be established by ion implantation.

EXPERIMENTAL:

$As^+$ ions of 1.8 MeV energy were implanted into a 25 μm thick Au foil to a dose of 6 X $10^{16}/cm^2$. The near-surface region of the target material contained about 5 at% As. The Au foil was connected to a sample holder which also acted as a thermal sink, the temperature of the target material thus being maintained to below 50°C. Following implantation the foil was thinned by 6 KeV $Ar^+$ ion etching. Etching was done on the back-side of implanted foil until a hole was formed (Fig. 1). The edges of the hole were examined in a Philips EM 300 TEM at an operating voltage of 100 KeV. The thicker sections of wedge obtained due to ion thinning could not be examined in conventional TEM because of the limitation on the penetration depth of 100 KeV electrons in Au. Therefore, HVTEM was employed at the New York State Health Department Laboratory and Research Division, Albany, N.Y. The microscope is a EM7 Mk II, which can be operated in the range of 100 KeV to 1.2 MeV. It has a stabilized beam power of 10 W; unstabilized irradiation (high current mode) up to 200 microamps, with the finest beam spot of 1000 Å. Resolution is about 4 Å, the theoretical resolution being 1.8-2.8 Å. Magnification up to one million can be obtained. In the present experiment 1 MeV electrons were used. Annealing studies were carried out in 100 KeV TEM by in-situ heating, the temperature being controlled with an accuracy of ± 25°C. Selected area diffraction patterns were analyzed with a microdensitometer.

RESULTS AND DISCUSSION:

The results with conventional TEM are shown in Figs. 2a and 2b, the diffraction rings corresponding to Au (111), Au (200), Au (220), Au (311) and As (102). The (102) reflection is the most intense line in the X-ray diffraction pattern for pure As, and, therefore, it is reasonable to expect the same here. The presence of pure crystalline As is indicated and this can be seen in the corresponding micrograph as black spots. The sizes of the As precipitates are in the range of 150-200 Å. As evidenced by the diffraction pattern,

implantation of a metalloid ion such as As into Au at 1.8 MeV did not result in diffuse rings which may be indicative of an amorphous structure.

In order to investigate the above, calculations were carried out on the depth of maximum damage induced by the impinging $As^+$ ion in the Au matrix, using the computer program developed by Mueller and Manning (7). In this program, an energetic heavy ion beam considered to penetrate and come to rest within an amorphous target. In determining the number of atomic displacements, Mueller and Manning found that crystalline effects are unimportant in polycrystalline cubic metals. Accordingly, the key quantity in determining damage is the profile of deposited energy as a function of penetration depth. The computer program was used to calculate such energy profiles.

From such calculations, we found that 1.8 MeV $As^+$ ions yield an energy profile peaking at about 2000 Å (Fig. 3). This indicates that most of the $As^+$ ions lose their energy in this vicinity in Au. A region of high disorder should be expected at this depth, perhaps resulting in a microcrystalline/amorphous structure. However, in conventional TEM the penetration depth of 100 KeV electrons in Au is no more than 500 Å, which implies that we are examining a region very near to the surface, and far removed from the location of maximum disorder.

Indeed, it is clear that the principally damaged region has been removed by sputter-etching. The region under observation is without much damage, and additionally there is considerable heat generation in this region due to electron-atom interaction during implantation. This heat would anneal out some of the damage giving rise to a polycrystalline structure in that region. This is confirmed both by the SAD pattern and the TEM micrograph (Fig. 2a and 2b).

HVTEM experiments were subsequently carried out to confirm the theoretical calculation from which we have expected to observe an amorphous/microcrystalline

layer. HVTEM has the advantage of greater penetration depth, making it possible to penetrate through the 3000 Å thick layer of implanted substrate. Fig. 4a shows the SAD pattern from a thick region. The presence of diffuse halos in the diffraction pattern suggests amorphicity or microcrystallinity. The corresponding micrograph shows a non-crystalline structure. No contrast is observed from the main crystalline phase due to the fact that the amorphous phase has scattered the central beam leaving an effective "beam" which has been diffused. Fig. 5 shows the SAD pattern of a region closer to the edge of the etch-formed hole (see Fig. 1), which clearly shows that the region is polycrystalline. The Au and As lines are easily identifiable. There is precipitation of or clustering of As in this layer similar to what is observed in Fig. 2b. It is thus seen that an amorphous/microcrystalline layer can be induced within a crystalline matrix on implantation to the MeV range.

ANNEALING:

Microstructural changes are observed on in-situ heating within the microscope. Initially, up to about 400°C there was not much change in the microstructure or in the SAD pattern. Above this temperature, the diffraction rings sharpened and new rings due to different planes developed as As precipitated out. Fig. 6 shows a microdensitometer trace of the diffraction patterns taken at different temperatures. Figs. 6a, 6b, 6c and 6d are the microdensitometer traces for SAD patterns at room temperature, 681°, 751° and 790°C (for 30 minutes), respectively. The gradual increase in the number of peaks and the increase in their intensity indicate the precipitation of As out of the Au matrix. Figs. 7a and 7b show the SAD pattern and micrograph of As precipitates at 790°C. The resulting hazyness is due to specimen stage movement at high temperature. Figs. 8a, b and c show bright and dark field images, and the SAD pattern of the As precipitates after cooling from 790°C to room temperature. These pictures are from HVTEM.

It is observed that even at high temperature, As is stable, even though the sublimation temperature of As is 613°C. Stability of this phase is found in the equilibrium phase diagram where the eutectic exists at 636°C.

In this study we have found an amorphous structure in the implanted matrix, embedded within a polycrystalline layer. It is of interest to compare our result with the recent findings of Kant et. al. (8). In their study, they implanted 50 KeV $Sb^+$ into an Al single crystal. They found no amorphous structure, but rather detected an Sb-Al intermetallic compound. In both cases, a metalloid ion of high atomic number was implanted into a F.C.C. matrix. This is consistent with rapid-quenching work from the literature, and enables us to develop this study along principles of metastable alloy formation.

References


1. J. A. Borders and J. M. Poate, Phys. Rev. B13, 969 (1976).
2. J. M. Poate, J. A. Borders, A. G. Cullis and J. K. Hirvonen, Appl. Phys. Lett., 30, 365 (1977).
3. S. P. Singhal, H. Herman and J. K. Hirvonen, Appl. Phys. Lett.
4. A. Ali, W. A. Grant and P. J. Grundy, Phil. Mag. B37, 353 (1978).
5. R. Andrew, Phil. Mag., 1153, (1977).
6. B. Gather and R. Blachnik, Z. Metallkde 67, 168 (1976).
7. I. Manning and G. P. Mueller, Computer Phy. Commu. 7, 85 (1974).
8. R. A. Kant, S. M. Myers and S. T. Picraux, J. Appl. Phys. 50, 214 (1979).

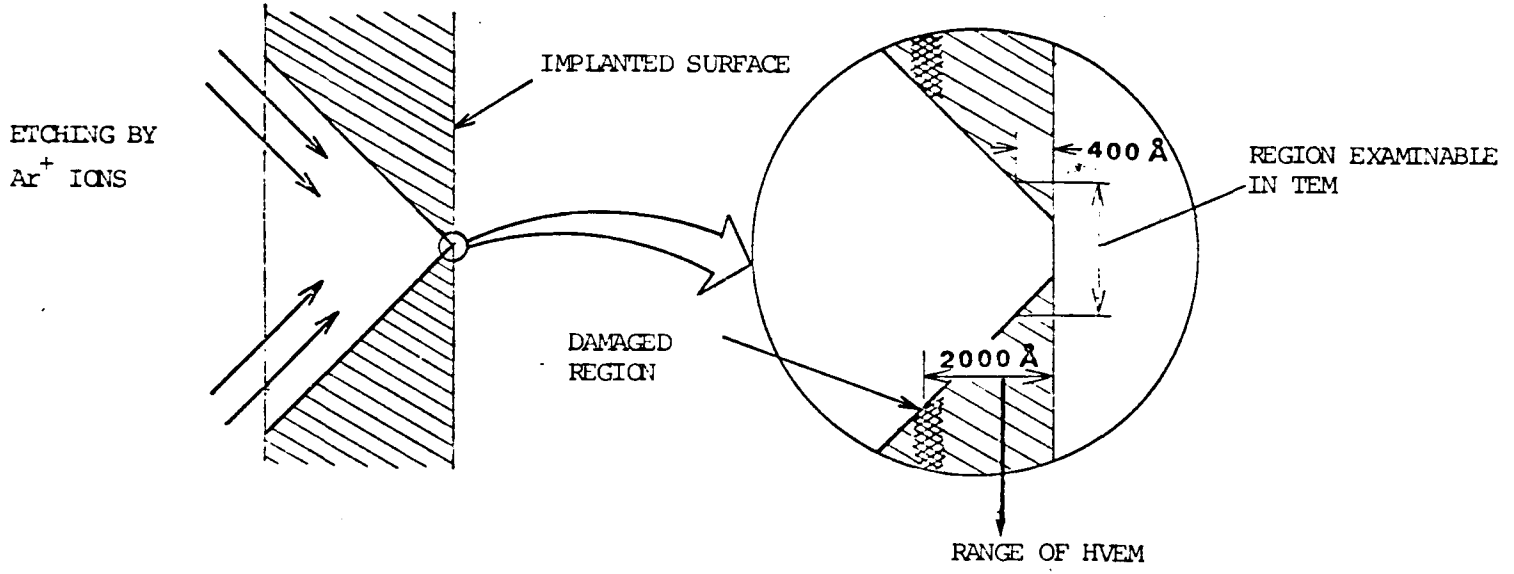


FIG.1. Argon ion etching of the implanted foil from the back side. (see text).

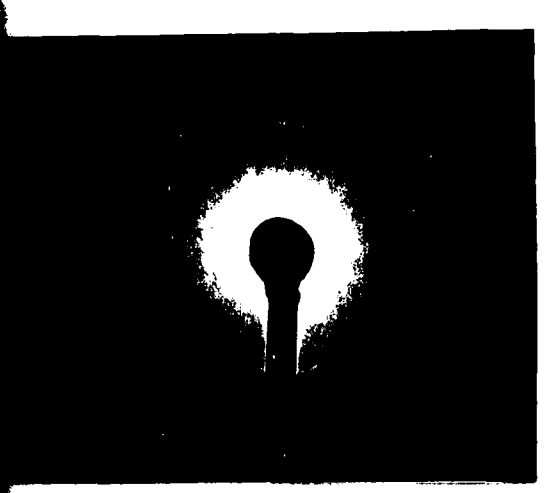

FIG.2a. SAD pattern of as implanted Au. Rings are identifi-( as Au(111), Au(200), Au(220), Au (311) and As(102).

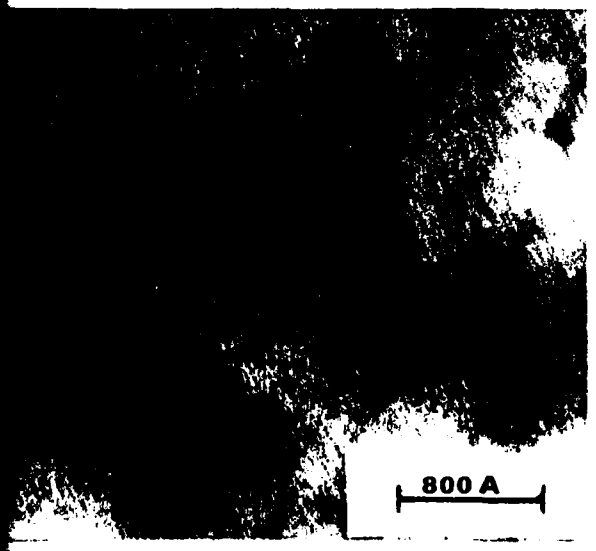


FIG.2b. Bright field image of As implanted Au. Micrograph from a region away from the damage peak. (Ref.Fig.3 & see text)

COMMAND-
CYCLE 5

FIG.3

As in Au

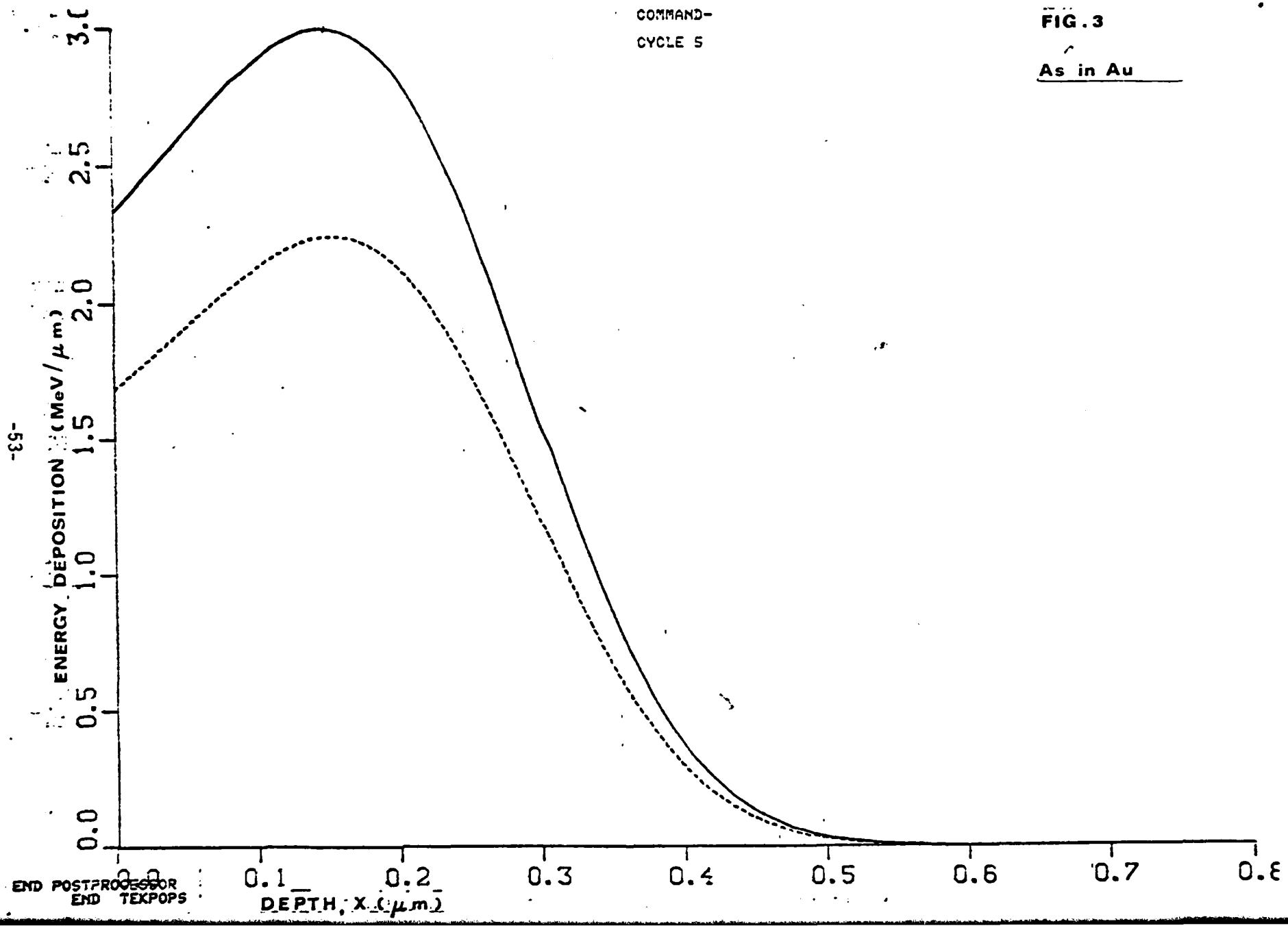


END POSTPROCESSOR
END TEXPOPS

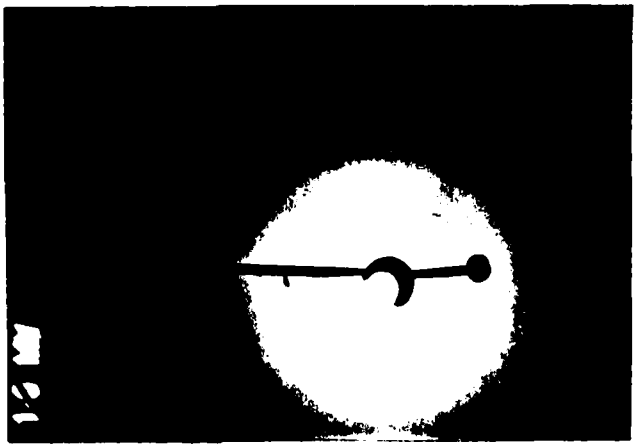

FIG.4a. SAD pattern from a thick region. Diffuse rings suggest microcrystalline/ amorphous structure

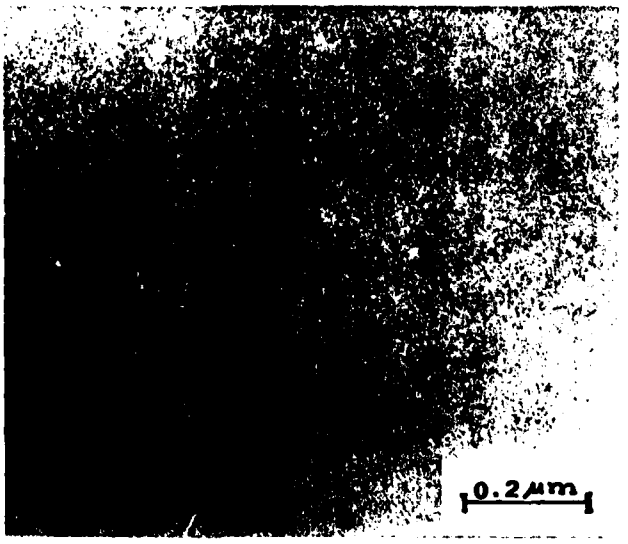


FIG.4b. Bright field image of a thick region with a SAD pattern as shown in fig.4a. Glassy appearence/no contrast

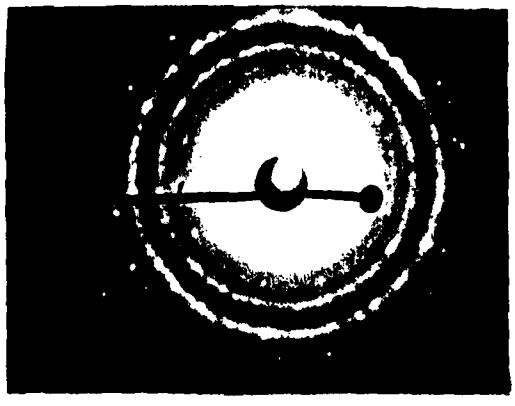

FIG. 5. SAD pattern from a thin region away from the damaged area. (SAD pattern from HVEM).

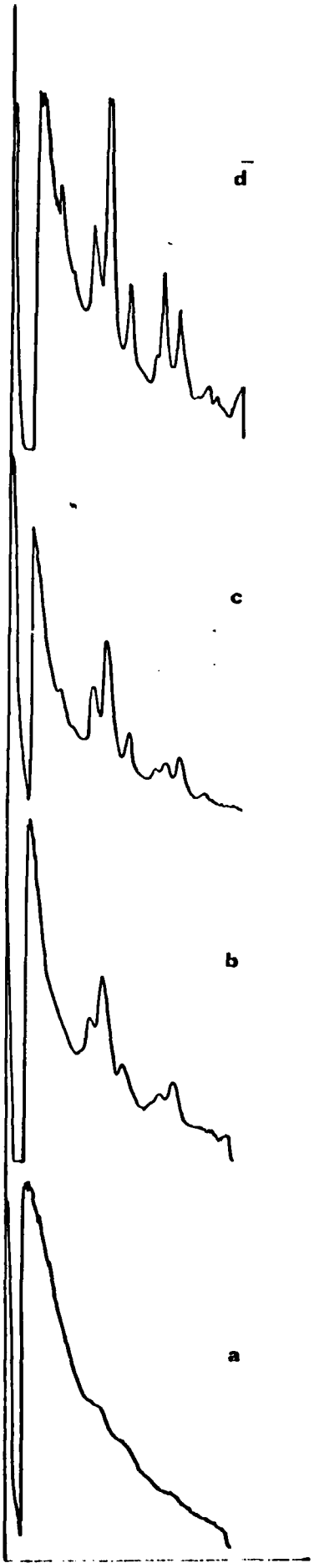


FIG.6. Microdensitometer traces of SAD patterns taken at
a. Room temperature,
b. 681°C
c. 751°C
d. 790°C

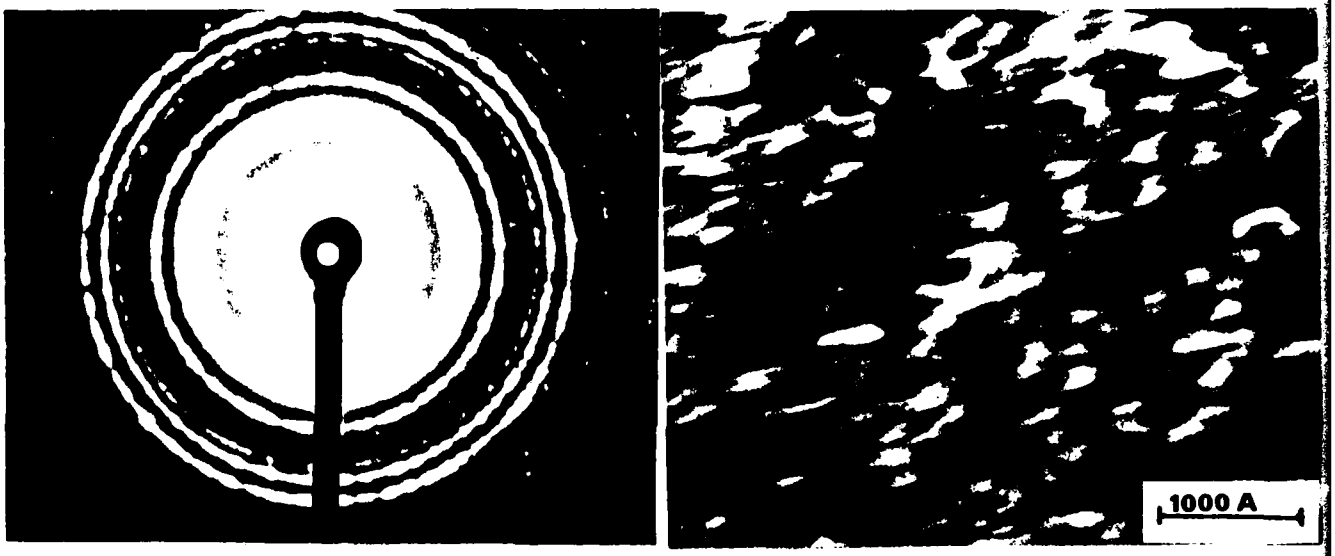


FIG. 7a and 7b. SAD pattern and bright field image of $As^+$ implanted Au; after 30 mins at 790°C.

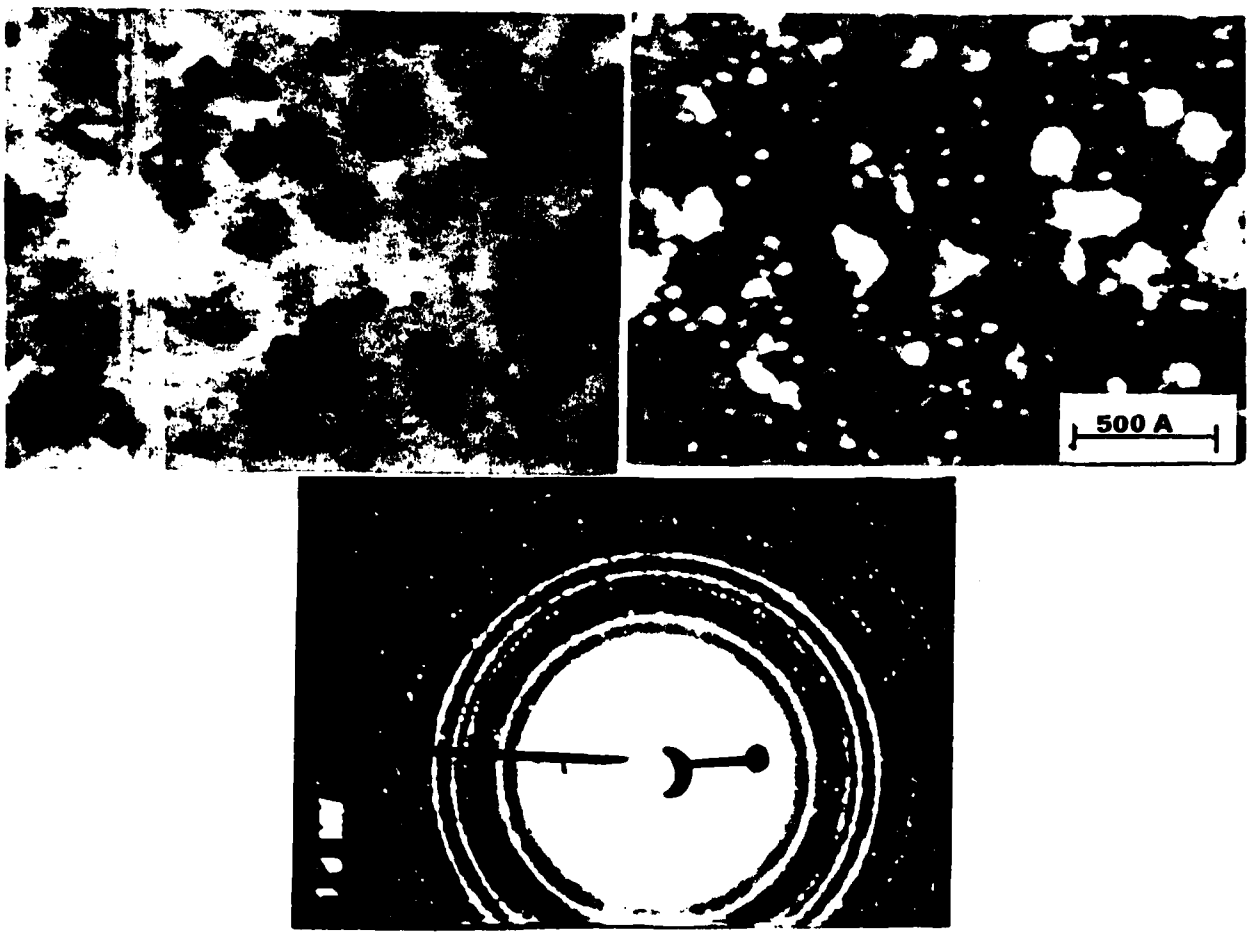


FIG. 8a, 8b & 8c: Bright field, dark field images and SAD pattern of As precipitates after cooling from 790° C.
(Images and pattern from HVEM)